POMS PRODUCTION AND OPERATIONS MANAGEMENT

PRODUCTION AND OPERATIONS MANAGEMENT

Vol. 30, No. 8, August 2021, pp. 2492–2521
ISSN 1059-1478 | EISSN 1937-5956 | 21 | 3008 | 2492
DOI 10.1111/poms.13393

Mobility-As-A-Service for Resilience Delivery in Power Distribution Systems

Dmitry Anokhin
Department of Decision Sciences, School of Business, The George Washington University, 2201 G Street NW, Washington, District of Columbia 20052, USA, danokhin@gwu.edu

Payman Dehghanian
Department of Electrical and Computer Engineering, The George Washington University, 800 22nd St. NW, Suite 6630, Washington, District of Columbia 20052, USA, payman@gwu.edu

Miguel A. Lejeune*
Department of Decision Sciences, School of Business, The George Washington University, 2201 G Street NW, Washington, District of Columbia 20052, USA, mlejeune@gwu.edu

Jinshun Su
Department of Electrical and Computer Engineering, The George Washington University, 800 22nd St. NW, Suite 6630, Washington, District of Columbia 20052, USA, jsu66@gwu.edu

Inspired by the opportunities provided by the Industry 4.0 technologies for smarter, risk-informed, safer, and resilient operation, control, and management of the lifeline critical networks, this study investigates mobility-as-a-service for resilience delivery during natural disasters. Focusing on effective service restoration in power distribution systems, we introduce mobile power sources (MPSs) as the restoration technology of the future, the mobility of which can be harnessed for spatiotemporal flexibility exchange and effective response and recovery during disasters. We present automated decision-making solutions that coordinate the MPSs utilization with repair crew (RC) schedules taking into account constraints in both energy and transportation networks. When integrated, the suggested technology aided by the proposed optimization models will have the potential to disrupt the current practice in boosting the resilience and operational endurance of the mission-critical systems and services during disasters, ultimately resulting in an enriched social welfare and national security.

Key words: mobile power sources; service restoration; transportation systems; disaster management; resilience
History: Received: September 2020; Accepted: February 2021 by Martin K. Starr and Sushil K. Gupta, after 1 revision.
*Corresponding author.

1. Introduction

This study investigates the effective utilization of mobile power source (MPS) technologies for resilience delivery in power distribution systems (DS) during extreme disasters. In section 1.1, we provide background information on several recent major natural disasters that led to prolonged electricity outages and emphasized the criticality of DS resilience. In section 1.2, we discuss the current practice and existing challenges in DS service restoration. Introducing MPS as a disruptive technological solution for effective response and recovery during natural disasters in section 1.3, we present, in section 1.4, a literature review on disaster management and the state-of-the-art on the use of MPS for DS service restoration. Eventually, the paper contributions and its structure are presented in section 1.5.

1.1. Motivation and Rationale

In recent years, there has been an increase in the frequency and magnitude of high-impact low-probability (HILP) events— which, according to recent statistics (National Academies of Sciences 2017), have resulted in excessive equipment damages, prolonged electricity outages, significant economic losses, and disruptions in our modern society (Zhang et al. 2019). In the United States in particular, a total of 70 weather-driven disasters occurred from 2015 to 2019 and resulted in billions of dollars of costs (National Centers for Environmental Information 2020). Figure 1 demonstrates the rising frequency of extreme natural disasters in the United States from 2016 to 2019 (Smith 2020), most of which led to extensive electricity outages. Seven major blackouts in the US history lasted between 10 and 50

Figure 1 Extreme US Natural Disasters from 2016 to 2019 (Smith 2020, National Centers for Environmental Information 2020) [Color figure can be viewed at wileyonlinelibrary.com]

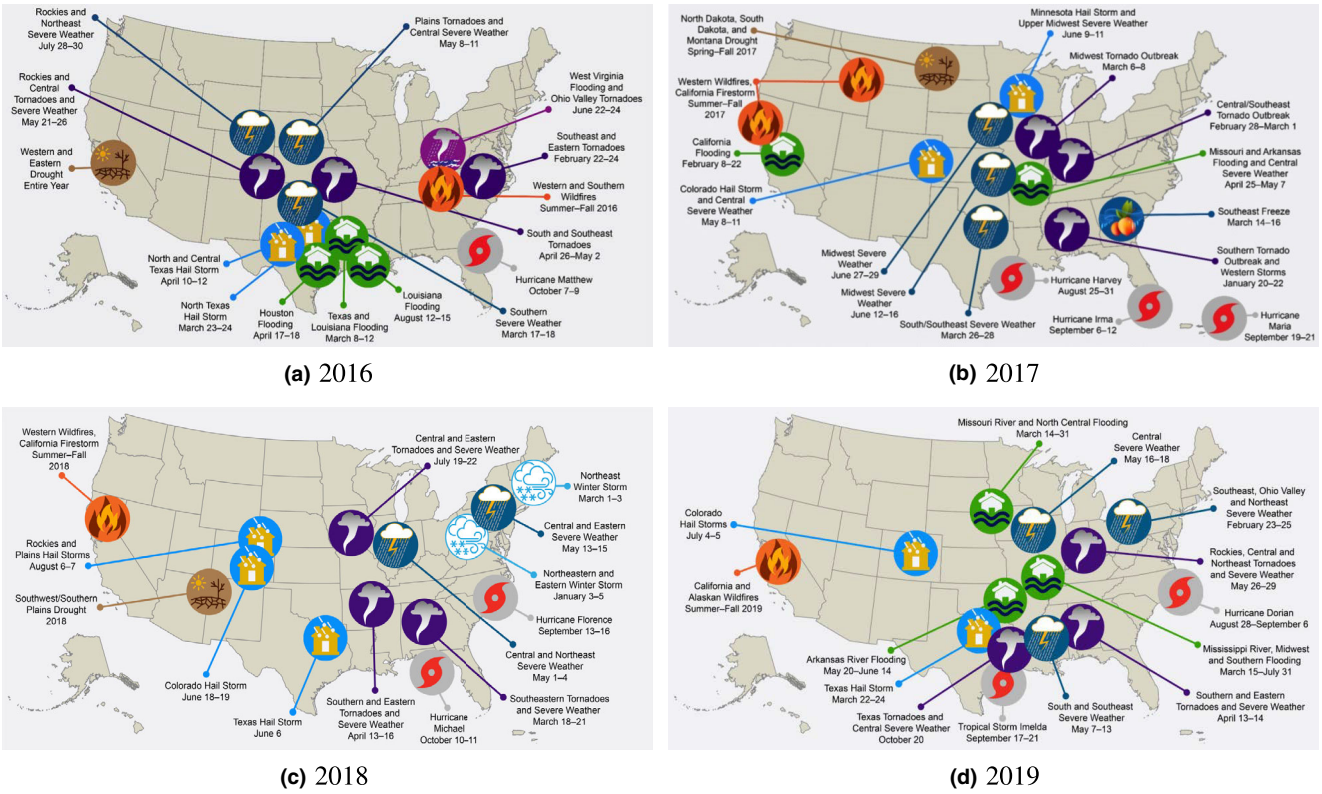

hours, with the associated costs exponentially increasing as the duration of the outage increases. Example events with major electricity outages are: (i) the 2017 Hurricane Harvey causing substantial electricity outages (around 10,000 MW) and leaving more than 291,000 people without power, (ii) the Hurricane Sandy in 2012 resulting in 10% of customers in New York and New Jersey without power for 10 days, $14 to $26 billion economic losses, and 50 deaths due to the sustained outage of electricity (National Academies of Sciences 2017); (iii) the Hurricane Maria in Puerto Rico in 2017 causing disruptions in 31 major power generating units in 20 facilities and leaving the entire island without electricity—the largest blackout in US history in terms of customer hours of electricity outage. Similarly, extreme weather events with extensive electricity outages have been trending higher globally. During the 2008 winter storms in Southern China, a nearly 2-week blackout resulted in 4.6 million people out of electricity, with 60 people losing their lives including 11 electricians working on service restoration (Bie et al. 2017). The Tohoku earthquake in 2011 in Japan impacted about 8.9 million households in 18 prefectures (Kuwata and Ohnishi 2011) while the 2017 Sarpol-e Zahab earthquake in Iran resulted in a city-wide blackout for weeks (Zare et al. 2017).

The energy system serves as the backbone for lifeline networks and drives a myriad of interdependent systems and mission-critical services, such as water, communication, transportation, health, military, and government sectors and services. When the electricity is out, water and communication systems may be disrupted quickly translating into a national security concern; various industries may halt for hours (if not days) resulting in significant economic losses; people in need of specific health care at home or nursing facilities would die due to the sustained loss of electricity supply that is essential for their health and well-being. With the need to sustain quality electricity supply to end-customers (particularly mission-critical services), safeguarding the nation's electric power grid and enhancing its resilience in the face of HILP incidents are the top priorities and have become increasingly critical for social welfare. Resilience refers to the ability of an electric grid to recover quickly and effectively following an HILP event and to adapt its operations and structure in order to mitigate the impact of similar events should they happen in the future (Panteli and Mancarella 2015). The concept of resilience is illustrated in Figure 2, where R_o and R_{pd} represent the resilience level of the system in normal and degraded operating states, respectively. Associated with an extreme weather event, an electric grid goes through

Figure 2 Concept of Resilience Against HILP Events [Color figure can be viewed at wileyonlinelibrary.com]

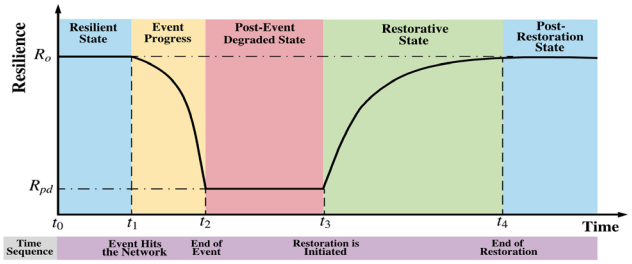

the following operating states: pre-event resilient state (t_1–t_0), degrading state while the event progresses (t_2–t_1), post-event degraded state (t_3–t_2), restorative state (t_4–t_3), and post-restoration state (after t_4).

We here discuss the bulk power grid and the facts that motivated us to gear our research direction toward solutions for resilience in the DS in particular. Figure 3 illustrates the general structure of the bulk power grid. A bulk power grid mainly consists of three hierarchical levels including generation system, transmission system, and the DS. The generation system owns different types of power plants (e.g., thermal and hydro power plants, wind farms, etc.) to produce electric power, mostly located far away from the demand centers. The generated electricity is transmitted over hundreds of miles through the transmission system from distant power plants to demand centers. In each demand center, a substation is located facilitating the transfer of electricity from the transmission system to the DS; the DS then brings the electricity to individual customers (e.g., homes, industries, commercial buildings, emergency services). While all three segments of the bulk power grid might be vulnerable to extreme events and environmental stressors depending on the nature and intensity of such events, the DS provides the last mile electricity connection to the end-consumers and is particularly vulnerable due to its radial topology (see Figure A.1 in Appendix A) and limited backup resources (Lavorato et al. 2012). Any disruption in the DS (e.g., equipment failure, natural disasters, cyber-attacks, etc.) may directly and swiftly translate into customer interruptions and power outages. With the increasing frequency and intensity of HILP events, it is primordial to deploy solutions for enhancing the DS resilience, that is, ensuring a continuous, secure, and reliable supply of electricity to end-use consumers, particularly mission-critical services.

1.2. Current Practice and Existing Challenges for DS Service Restoration

Service restoration decisions, disruptions in power production, and DS operations in facing extreme events have posed serious challenges for decades. In practice, power restoration following an extreme event is commonly approached through (i) maintenance and repair activities of the damaged infrastructure by repair crews (RCs), (ii) switching actions and network topological reconfiguration to alter the electricity flows for faster electricity service restoration, and (iii) deployment and use of stationary emergency generators (SEGs) installed at critical load points as a backup energy source during emergencies.

In the first strategy, the repair process may take days, leaving thousands of people without electricity until the damaged equipment is fully repaired and returned back online. The duration of the repair process can vary depending on the geographical area (rural or urban), nature and intensity of extreme events, human resource and RC availability, and disruptions in other interdependent critical infrastructures, such as communication and transportation systems (TSs). The prolonged electricity outage due to lengthy repair processes may result in dramatic consequences to people and every aspect of our electrified economy. Although the second practice, that is, network topology control, can be performed in an automated manner, this practice requires the installation of switching infrastructure (i.e., switches, breakers) across the DS to enable network topological reconfiguration via opening/closing of the switches. While many DSs in practice may not be equipped with the required number of switches, making the DS fully re-configurable through the installation of switching infrastructure is an expensive option that needs to be incorporated in expansion planning studies by DS planners. Moreover, the switching infrastructure could be also damaged due to the HILP incidents or could become unavailable due to poor maintenance of equipment over time. Unlike the first and second approaches—which contribute to the entire DS restoration through grid-scale re-connection or reconfiguration—backup SEGs are employed to supply power locally to particular services following extremes, such as providing electricity for hospitals to rescue injuries or energy-intensive flood water pumping facilities. The contribution of backup SEGs is in general limited. Furthermore, SEGs produce electricity by consuming diesel fuels, and their effectiveness will be hindered by potential disruptions in the fuel supply chain and transportation sector during HILP events. This motivates us to propose and search for a new disruptive technology that can aid in (i) facilitating a faster DS restoration and its sustained operation during HILP events and (ii) supporting the energy-intensive facilities (e.g., flood water pumping), as well as the electricity delivery to mission-critical systems and emergency services until the system is returned to its normal operating condition.

Figure 3 General Structure of the Bulk Power Grid (Fortis Alberta 2019) [Color figure can be viewed at wileyonlinelibrary.com]

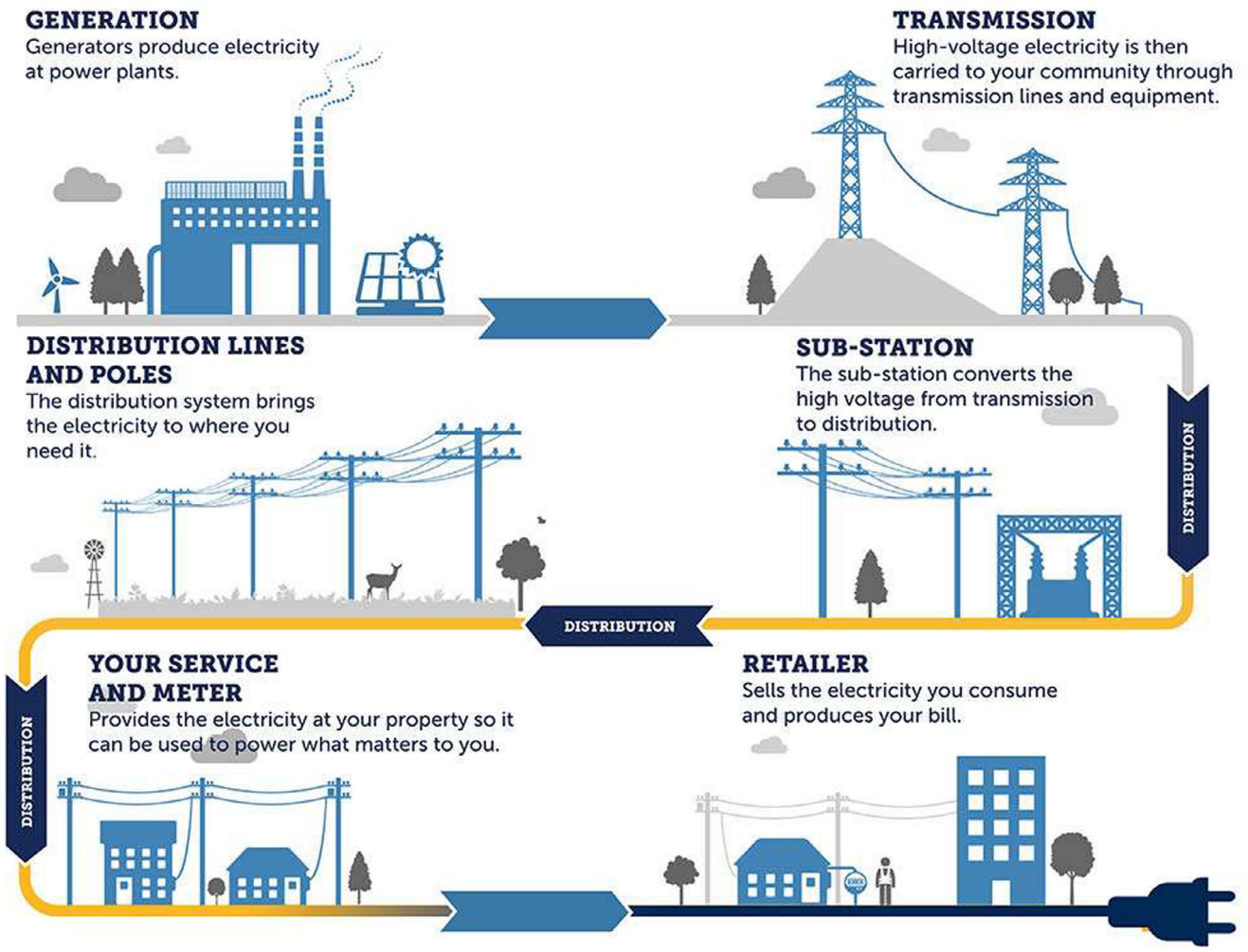

1.3. Mobile Power Source: A Disruptive Solution for Resilience Delivery in DS

Besides the three approaches mentioned above, a new technology has recently gained increasing attention for enhancing the DS resilience and operational endurance during and following HILP events—mobile power source (MPS). MPSs are emergency service vehicles, including mobile energy storage systems (MESSs) and mobile emergency generators (MEGs), the mobility of which could be harnessed during extreme events to deliver spatiotemporal flexibility exchange and enhance the DS resilience. More specifically, spatiotemporal flexibility refers to the feature of MPSs being able to travel across space and time, that is, to deliver power and energy via the TS during the restoration process (Lei et al. 2019b). MPSs can be one of the most effective response and recovery resources when sustained damage leads to prolonged electric service outages in the DS. Complementary to backup SEGs, MPSs are portable and can travel through the TS to reach the critical nodes as the damaged infrastructure are being mended by RCs. In urban areas, it generally takes several hours for RCs to repair a DS infrastructure, while RCs might spend days in rural areas until the damaged infrastructure is fixed. In coordination with the RC schedules, the DS restoration process can be accelerated by assigning MPSs to serve the system's critical load points. Since MPSs are emergency service vehicles, they should be dispatched to required areas through the TS. The node-to-node connectivity status of the TS should be carefully taken into account when deciding on the joint assignment of MPSs and RCs for DS restoration. This is because HILP events (e.g., earthquake, ice storm) may disrupt the TS (i.e., travel route availability), which impacts the decisions on routing and scheduling of MPSs and RCs during the restoration process. For instance, if the shortest path in the TS to reach a critical load point is disrupted, decision-makers need to dispatch MPSs through a "second" shortest path. Hence, restoration strategies with joint utilization of MPSs and RCs should be coordinated across the DS and TS.

While MPSs can accelerate the response and recovery of the DS in the face of HILP events, their potential for delivering resilience services has remained largely untapped and they are currently not well utilized in practice. For example, before Hurricane Sandy struck (Barrett 2012), 400 industrial-size MPSs were prepared by the Federal Emergency Management Agency (FEMA), but only a portion of them was providing power even three days after Sandy made its landfall. Holistic strategies enhancing the efficiency of MPSs utilization can render faster restoration and augmented resilience.

1.4. Literature Review

Disaster management has long been the focus of researchers in operations research and management (Altay and Green III, 2018, Arnette and Zobel 2019, Balcik et al. 2019, Gupta et al. 2016, Lorca et al. 2017, Ni et al. 2018, Pan et al. 2020, Parker et al. 2019, Sodhi and Tang 2014, Stauffer and Kumar 2021, Ye et al. 2020a). Driven by Industry 4.0/5.0 technologies (Faheem et al. 2018, Ivanov 2018, Schwertner et al. 2018), the ability of an electric grid to recover quickly and efficiently following an HILP event can be improved dramatically with the use of MPS technology. Disaster management to respond to natural extremes (Henry and Ramirez-Marquez 2016) and to man-made cyber attacks (Nguyen et al. 2020) affecting power grids has been researched quite extensively over the last decade. We present approaches used in power grids to build up resilience against weather-driven extreme events.

We first review studies where attempts were made to apply MPSs to enhance the resilience in power systems. Lei et al. (2016) proposed a mixed-integer linear programming (MILP) problem to minimize the outage duration of loads by dispatching MEGs to outage nodes. A resilience-driven response plan to mitigate the damage and socio-economic losses after a natural disaster was developed by Kim and Dvorkin (2018). The proposed two-stage stochastic problem determines the transportation of the MESSs from their stationary locations to the outage nodes taking into consideration the routing decisions with topology switching and microgrid formation. Lei et al. (2019b) set up an MILP post-disaster restoration model to enhance the DS resilience by scheduling MPSs in coordination with DS reconfiguration. A two-stage robust optimization model with routing and scheduling of MPSs was proposed by Lei et al. (2019b) for DS resilience enhancement. A rolling integrated service restoration strategy through scheduling and routing MPSs is introduced by Yao et al. (2019). Their two-stage stochastic MILP problem coordinates the MESS fleet in microgrids to minimize the total system cost with uncertainties in the transportation network connectivity and the damaged branches.

Another approach—the use of RCs to fix the damaged infrastructures in the DS following an HILP event—has been investigated in several studies. A co-optimization approach was introduced by (Arif et al. 2017) to handle, in a decoupled manner, the DS restoration-reconfiguration and RCs' routing problems. A joint switch operation, crew dispatch, and component repair approach for DS restoration was introduced by Chen et al. (2019) and demonstrated the benefits of dispatching RCs by coordinating switching operations and components repairs. The RC dispatch problem for combined electric and natural gas systems operations was introduced by Lin et al. (2019). Their MILP model minimizes the cost of electric load shedding, gas load shedding, and the total repair duration. Zhang et al. (2020) proposed a model for disaster recovery by integrating the dispatching of the maintenance and restoration crews to pre-assigned damaged components in order to enhance the DS resilience.

Complementary to past research, some references studied MPSs routing and scheduling jointly with RCs. For example, Arif et al. (2016) proposed a co-optimization model for the repair and restoration of power transmission systems. They took into account the load points' priorities and developed an MILP model to coordinate generators' dispatch and RCs and to maximize the amount of the restored power. Lei et al. (2019a) introduced a co-optimization method for disaster recovery logistics to enhance DS resilience. The proposed mixed-integer nonlinear programming model maximized the weighted sum of the restored loads over time with the joint routing and scheduling of RCs and MPSs coordinated with the dynamic DS network reconfiguration. Xu et al. (2019) proposed a linear multi-period DS restoration model taking into consideration the travel time of MPSs and RCs, and the repair time of the damaged components. Ding et al. (2020) developed an MILP for multi-period DS restoration that maximizes the total weighted loads restored. Ye et al. (2020b) proposed a model to dispatch MPSs and RCs with the objective of improving the restoration process in unbalanced DS.

This literature review illustrates the complexity of the disaster management decisions in DS following HILP events and the difficulty to effectively deploy and coordinate MPSs and RCs to enhance system resilience. Most studies in the extant literature on MPS allocation and dispatch for resilience delivery focus solely on the impacts of deploying MPSs in the electrical network, that is, the electricity outage recovery and service restoration, with no consideration to other available resources (e.g., RCs) and the interdependent TS availability during disasters. In particular, Lei et

al. (2016), Kim and Dvorkin (2018), and Lei et al. (2019b) investigated the application of MPSs-only solutions for DS restoration; Arif et al. (2017), Chen et al. (2019), Lin et al. (2019), and Zhang et al. (2020) presented DS restoration through RCs-only approaches without taking MPSs into account. Studies on the coordinated routing and scheduling of RCs and MPSs for DS resilience (Ding et al. 2020, Lei et al. 2019a, Ye et al. 2020b) did not consider the TS availability. Moreover, a few studies that capture the interdependence of the electrical power DS and TS use a decoupled (hierarchical) approach to address the complex resilience optimization problem across the two networks. That is, the resources in one system (e.g., TS) are independently optimized and iteratively transferred to the other (e.g., DS). For example, in study Xu et al. (2019), the transportation routes and travel time of MPSs are first determined by solving the weighted dynamic traffic assignment problem in the TS in Step 1 and the multi-period load restoration strategy in the DS is determined in Step 2 based on the results in Step 1 (i.e., using the decisions taken in Step 1 as fixed inputs/parameters to solve the problem in Step 2). Such an approach calls for the "iterative" exchange of status information at each time period and decisions between the TS and DS operators through communication channels. This practice is vulnerable to communication failures and latencies which are not uncommon during disasters, further resulting in delayed attainment of the optimal recovery solutions, delayed utilization of resources for service restoration, and prolonged electricity outages amid an HILP incident. Additionally, such a frequent exchange of information (Xu et al. 2019) is vulnerable to cyber intrusions where the exchange of data between the system operators in TS and DS may be manipulated by cyber intruders, which may compromise the accuracy and fidelity of the response and recovery decisions in both networks. These issues and gaps motivate this study, the contributions of which are presented below.

1.5. Contributions and Paper Structure

Beyond the state-of-the-art models and literature, this study provides the following contributions:

1. We propose the concept of *mobility-as-a-service* for resilience delivery in the DS. Different from the vast majority of literature on the use of single-resource optimization for DS resilience, the proposed models aid system operators to make informed decisions on coordinated operations of MPSs and RCs for spatiotemporal flexibility exchange and resilience enhancement in the DS.
2. The proposed models effectively integrate the DS and TS constraints into *one joint formulation* allowing for globally and coordinated optimal solutions on routing and scheduling of MPSs/RCs for improved DS resilience. Different from the state-of-the-art, our joint optimization framework captures the status information of both DS and TS networks only once and coordinates the existing resources for effective service restoration. Relaxing the need for multiple and iterative exchanges of data and decisions between the two networks, the suggested approach minimizes the risks of communication failures/latencies and cyber-attacks during service restoration, which otherwise would impede timely and reliable decision-making for resilience.
3. Our extensive numerical and scenario-based investigations of the proposed models on mobility-as-a-service for resilience provide managerial insights on how to coordinate the available resources for effective response and recovery decisions against HILP events. Such considerations include the analyses of (i) different combination of existing MPS technologies —MESSs and MEGs, (ii) the conventional practices for DS restoration—RCs and SEGs, and (iii) different repair schedules to mend the damaged branches in the DS and give insights on the most productive utilization of MPS technologies for service restoration processes.

The remainder of the study is structured as follows. Section 2 describes the MPS technologies, their connection with Industry 4.0 technologies, and how they can potentially be of benefit for response and recovery to extreme HILP events. Section 3 describes the proposed multi-period models for routing and scheduling of MPSs and RCs and discusses their main characteristics and constraints. Section 4 describes the tests conducted to evaluate the efficiency and benefits of the proposed models in delivering resilience services. We summarize the managerial insights and concluding remarks in section 5.

2. Mobile Power Source in the Industry 4.0/5.0 Era

We describe the different industrial revolution phases in section 2.1 with the corresponding milestones and achievements. In section 2.2, we elaborate upon the Industry 4.0 and Industry 5.0 advancements and the opportunities provided for further technological innovations. section 2.3 sets forth how beneficial disruptive MPS technologies can be in the Industry 4.0 setting and in delivering resilience services in the face of extreme HILP events. We further discuss the new functionalities and future opportunities for MPSs

envisioned by the rapidly growing Industry 4.0 technologies as they evolve.

2.1. Phases of Industrialization

In pace with constant technological developments, industrialization's progress spans across five distinct phases. The first major breakthrough in the industrial revolution started at the end of the 18th century and brought about drastic industry mechanization in several sectors, including the transformation in the agricultural sector and the invention of the steam engine. In turn, this fueled the development of the railroad system and provided new means for economic acceleration. The second industrial revolution came about the end of the 19th century and was spurred by advances in the utilization of new energy sources, such as oil, gas, electricity, and the development of internal combustion engines. Other notable markers of the second revolution include steel developments, the rapid evolution of chemical synthesis, and the introduction of novel communication interfaces (i.e., telephone and telegraph). Perhaps the most significant products of the second industrial revolution were the automobile and the plane. Given the depth of change these products introduced to society, the second industrial revolution is often seen as the most important one in history. The third industrial revolution came in the second half of the 20th century, and is commonly associated with another source of energy—nuclear—and the rise in technological advancements in several new industries, including electronics, telecommunications, and computers. The third revolution brought about the exploration of space and biotechnology. Two major inventions, programmable logic controllers and robots, ushered in the era of high-level automation. The fourth industrial revolution, the so-called Industry 4.0, has yet to run its course fully, and is primarily driven by advances in the Internet. Along with the development of new industries and transformations in many of the existing ones, Industry 4.0 brought about the world of virtual reality. This naturally develops into Industry 5.0 with the rapid development of information and communication technologies, artificial intelligence and robotics, cyber-physical systems, and the ever more powerful Internet of things solutions. Industry 5.0 implies the growing cooperation between machines and human beings, and the ability to efficiently create personalized products at previously unattainable levels.

2.2. Industry 4.0 and Industry 5.0 Technologies

The term Industry 4.0, introduced in 2011 at a trade fair in Germany, refers to the fourth industrial revolution that has occurred in manufacturing (Liao et al. 2017). Industry 4.0 is generally defined as "*the integration of complex physical machinery and devices with networked sensors and software, used to predict, control and plan for better business and societal outcomes*" (Hermann et al. 2016). In other words, Industry 4.0 is the ongoing transformation of the traditional manufacturing and industrial practices combined with the latest smart technologies (see Figure 4). The German government defined the following strategies for Industry 4.0: "*the strong customization of products under the conditions of highly flexible production*" (Schwab 2017). Such an ideology implies a seamless integration between manufacturing operations systems and information and communication technologies, such as the Internet of things and machine to machine capabilities forming what is known as cyber-physical systems (Dalenogare et al. 2018, Frank et al. 2019, Tang and Veelenturf 2019, Wang et al. 2015). The required automation technology within Industry 4.0 is improved by the introduction of methods of self-optimization, self-configuration, self-diagnosis, cognition, and intelligent support of workers in their increasingly complex work environments. Industry 4.0 has attracted a lot of attention from both industry and academia. Compared to the third industrial revolution, Industry 4.0 spreads across every industry in every country at an exponential pace. The opportunities for billions of people connected through mobile devices, with unprecedented processing power, storage capacity, and access to knowledge, are unlimited. The velocity and scope of these changes herald the transformation of the entire systems of production, management, and governance. Industry 4.0 technologies highly impact fields including robotics, quantum computing, industrial Internet of things, fifth-generation wireless technologies, energy storage, and fully autonomous vehicles (Olsen and Tomlin 2020).

The term Industry 5.0 was first introduced in 2015 in "From Virtual to Physical" study (Rada 2015) published within the LINKEDIN social network. Adding a personal human touch to the Industry 4.0 pillars of automation and efficiency, Industry 5.0 is set to focus on the return of human hands and minds into the industrial framework (see Figure 4). Industry 5.0 primarily refers to the revolution in which man and machine reconcile and find ways to work together to improve the means and efficiency of production. Aimed at supporting—not superseding—humans, it can be manifested through robots helping humans work better, safer, and faster by leveraging advanced technologies like the Internet of things and big data to enforce the value of human intuition and problem-solving capabilities. Importantly, the fifth revolution has well pronounced social and sustainability dimensions as companies increasingly emphasize clean renewable energy sources and waste elimination.

Figure 4 Focused Technologies in (a) Industry 4.0; (b) Industry 5.0 [Color figure can be viewed at wileyonlinelibrary.com]

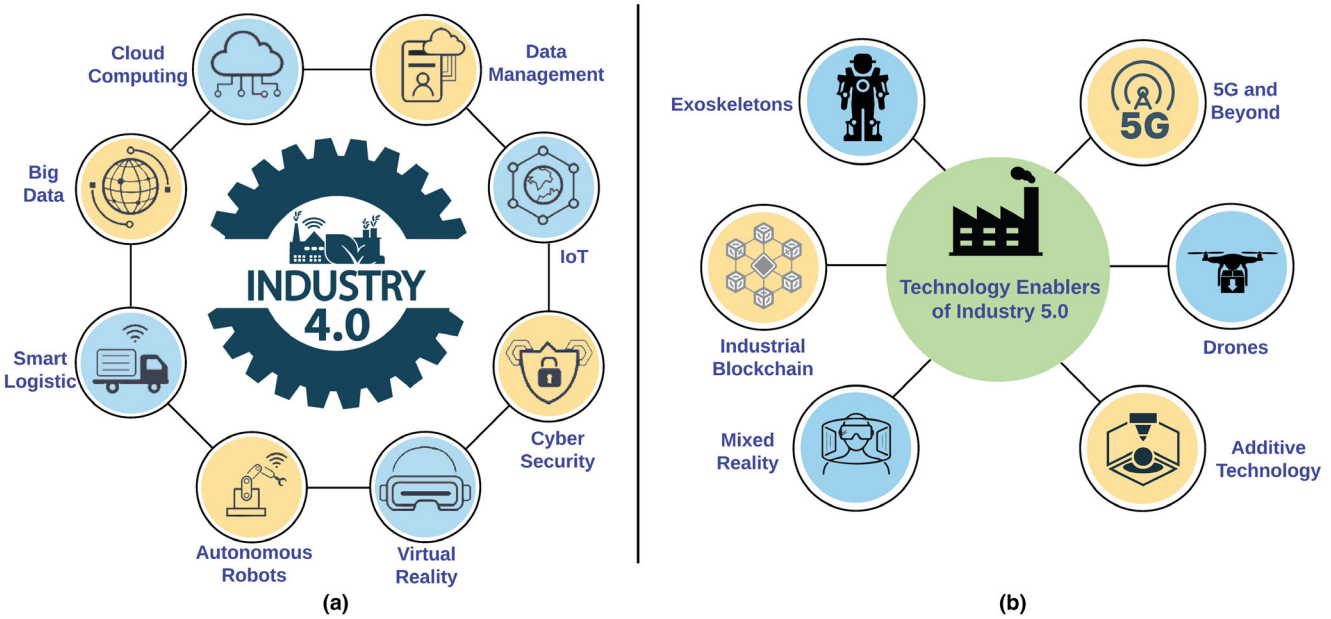

2.3. Mobile Power Source Technology in an Industry 4.0 Setting

The availability of Industry 4.0 technologies provides opportunities for automation of MPSs priority services with the goal to strike a balance between machines and humans working hand-by-hand during the service restoration process consecutive to an HILP event. The analytical framework introduced in this study integrates major elements—including data-collecting sensors, MPS units, and physical infrastructure components in both DS and TS—to improve business continuity and societal endurance during disasters. The proposed technological solution in this study, as well as the future machinery innovations in self-driving cars and unmanned MPS, clearly fall under the Industry 4.0 purview as defined by Hermann et al. (2016). In particular, such technological and analytical advancements could be used in an automated driving system and self-driving cars, offering great, and yet untapped potential, if applied to MPS technologies of the future. Advancements in artificial intelligence will help make MPSs autonomous with significant applications in harsh environments and will allow MPSs to act as technical assistants to the human workforce in tasks that are complex in nature or unsafe. Different from the existing MPS technologies relying on human drivers, autonomous MPSs of the future will relax the need for excessive human resources needed in such services, particularly during extreme HILP events and in case of human workforce shortages. Additionally, Industry 4.0 technologies enable advances in materials sciences and high-performance high-capacity energy storage designs that could bring the use and efficiency of MPS into new levels for resilience delivery in DS. Future application of MPS is envisioned to be realized through aerial means of transportation particularly in areas with either limited or disaster-disrupted transportation connectivity and access.

During the past several years, MPSs have been found to be new disruptive technologies and key enablers for DS outage management following HILP disasters. There are four main types of MPSs: electric vehicle fleets (EVs), truck-mounted MESSs, MEGs, and mobile wind turbine (MWT) generators:

- **MEGs** are critical flexibility resources for fast electric service restoration across the DS, especially when customers lose access to the main grid which is often the case following a natural disaster. MEGs are truck-mounted generators with the merits of mobility and large capacity (up to several MVA). They can be one of the most effective response resources for mission-critical systems and services when sustained damage leads to prolonged electric service outages in the DS.
- **MESS** is a utility-scale storage bank (e.g., lithium-ion battery) fully controlled by utility companies. Unlike stationary energy storage units, an MESS can be mobilized by a big truck and connected to the system to provide electricity to critical infrastructures and local services. Their transportability allows for spatiotemporal flexibility exchange and to deliver a localized power support, power losses reduction, voltage regulation, and integration of renewable energy sources.

- **EVs** can be charged to store energy, not only to meet its own transportation requirements, but also as an emergency power source to supply electricity to critical loads during emergencies. Previous research has demonstrated the benefits of EVs, if aggregated, in feeder-level capacity enhancement and resourcefulness for improving the DS resilience (Jamborsalamati et al. 2020). Charging and discharging of EVs can be facilitated through ongoing and future advancements in vehicle-to-grid, vehicle-to-building technologies, and EV charging infrastructure (Kahlen et al. 2018, Qi and Shen 2019, Valogianni et al. 2020).
- **MWTs** are transportable small-scale wind turbines that can unlock many applications in commercial, residential, government, military, and humanitarian markets. The MWT is purposely designed to extract as much energy as possible from wind and keep parasitic losses to a minimum during the delivery process. Beyond low-cost power, the machine will be invaluable for disaster relief efforts, in particular in rural areas, and other mobile operations that are constrained by the limitations of the power grid and/or availability of fuels. With the proliferation of distributed renewable energy resources globally, MWT offers a great opportunity in delivering resilience and other ancillary services to the DS of the future (Angelus 2020, Golari et al. 2017).

Among the aforementioned types of MPSs, we focus in this study on MESS and MEG. This choice of MPS technologies is supported by the following: (i) the focus of this study is on grid-scale service restoration following HILP events, while individual EVs do not have enough capacity to support the grid beyond one or multiple buildings, (ii) contrary to urban settings with high-rise buildings, MWTs can best release their potential in rural areas where wind availability is not compromised. Additionally, the ability to transport wind turbines adds additional complexities as the exogenous sources of uncertainty spatiotemporally moves. We do not consider MWTs in this study to keep the proposed models generic and applicable to DS of different structures and in different geographical areas.

3. Mobile Service Optimization (MSO) Models

In this section, we formulate and analyze mobile service optimization **MSO** models in the DS with considerations of the TS's availability and restrictions during disasters. After a brief and general description of the problem in section 3.1, we investigate the deployment of the MPS technologies for enhanced DS resilience to HILP incidents from two different perspectives: the minimization of the number of time periods needed for full service restoration—that is, **MSO** for minimal restoration time (**MSO-MRT**) in section 3.2.1—and the minimization of the total amount of power outage during the restoration process—that is, **MSO** for minimal loss of power (**MSO-MPL**) in section 3.2.2. In section 3.3, we present the service and system constraints common to both models. Model strengthening through deriving valid inequalities is presented in section 3.4.

The two models take the form of MILP problems and are discrete-time multi-period optimization models decomposed in periods of equal duration. They provide an integrated decision-making process as decisions regarding power generation, power restoration, and operations in the DS and TS networks are jointly and concurrently determined through the solution of a single optimization problem. This must be contrasted with earlier studies (Arif et al. 2016, 2017, Lei et al. 2019a, Zhang et al. 2020) that determine (some of) these decisions using a decoupled approach in which the outputs (decisions) of one model are used as inputs (parameters) in another one.

3.1. Problem Description

Figure 5 represents the overall architecture of the proposed work using the **MSO-MRT** and **MSO-MPL** models: the routing and scheduling of RCs and MPSs for DS restoration in order to fulfill the above-stated objectives. Service restoration following an extreme event requires making complex decisions on the assignment and deployment of the MPSs and RCs in the TS, and on identifying the most effective strategy in the DS. The status of damaged branches in the TS may significantly impact the dispatching schedule of MPSs and RCs, and further affects the restoration process in the DS. While prior research mostly assumes that MPSs can reach the damaged nodes directly and as needed (Arif et al. 2016, Lei et al. 2019a, Lin et al. 2019), this assumption is not always valid in real-world practices. The restoration process is facilitated by the flexibility of MPSs, which can be connected to any suitable node in the TS, usually close to the outage nodes in the DS. Yet, for such flexibility to ensure efficient restoration, it is critical to account for the interdependence of the TS and DS since it is not uncommon for the roads to be disrupted when the HILP event occurs or due to poor maintenance. Additionally, MPSs and RCs are typically dispatched through the shortest paths to enhance resilience. When the TS is disrupted, finding alternative shortest paths for both services simultaneously is particularly complex. The shortest path in TS may not be always

Figure 5 RC/MPS Scheduling During Service Restoration Process [Color figure can be viewed at wileyonlinelibrary.com]

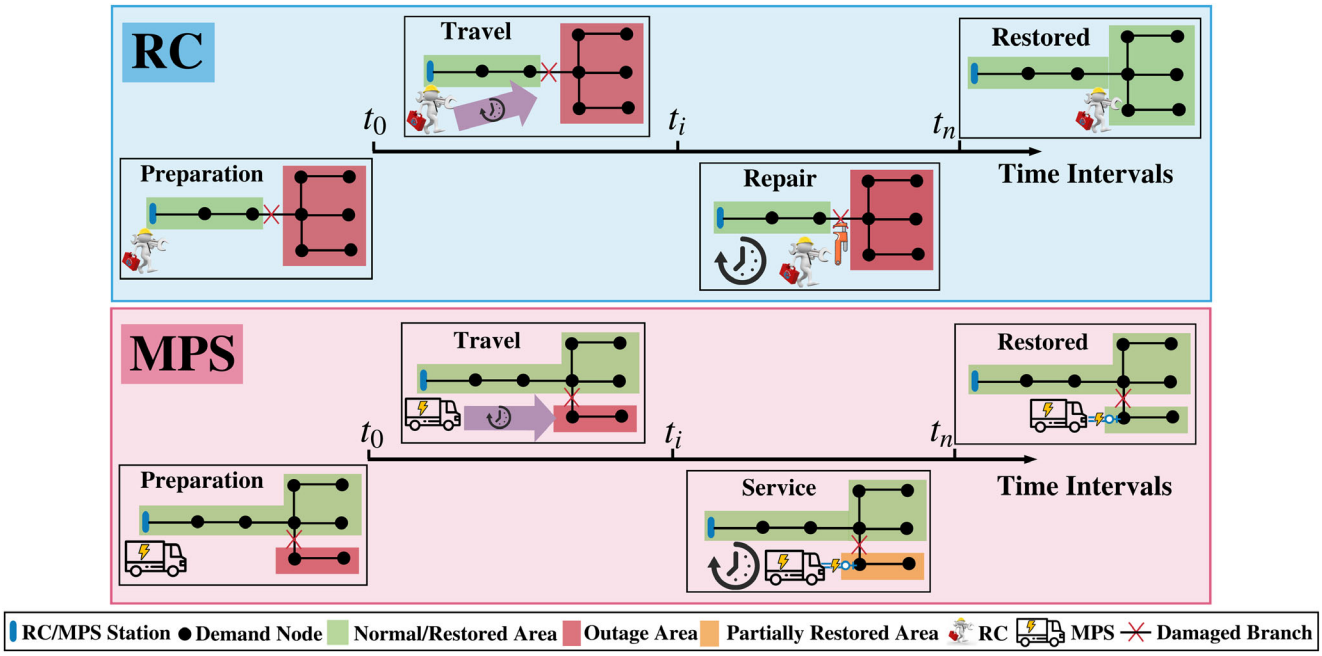

available due to the traffic congestion, or the active involvement of other emergency services (evacuations, firefighting, hospitalization processes, etc.). It is, therefore, essential to lift the assumption of TS and DS congruence and identify mechanisms to analyze the interconnectivity of the two systems to obtain the most effective restoration strategy. We demonstrate this with our numerical results in the next sections.

When an HILP event occurs resulting in electricity outages in the DS (i.e., damaged branches disconnect several nodes in the DS to the main source of power supply), the operator in RC/MPS station must decide to assign an RC to repair the damaged branch. The RC is ready to provide service in the initial time period t_0 and to travel along the TS to the location of the damaged branch. The RC then arrives at the location of the damaged branch at time t_i and repairs the damaged branch until t_n. When the damaged branch is mended by the RC at time t_n, the entire DS is fully restored. Similarly, when the outages occur in the DS, an MPS is assigned from RC/MPS station to the outage node in the initial time period t_0. It takes $t_i - t_0$ time periods for the MPS to travel and reach the outage area in the DS. The MPS then spends $t_n - t_i$ time periods to deliver power to the outage node and restore service. At time t_n, the service is fully restored in the DS. Both the RC and the MPS stop their activities once service is fully restored.

3.2. Model Formulations

Two **MSO** models proposed in this study take the form of multi-period MILP models and are challenging to solve due to their size and the many combinatorial and logical requirements. Both models differ in their objective functions and in a subset of constraints needed to represent the conditions with which a specific objective is accurately represented. The presentation is accordingly structured in two main parts. The first part—sections 3.2.1 and 3.2.2—presents the idiosyncratic components (objective function and corresponding specific constraints) of the two models. The second part—sections 3.3.1 to 3.3.7—describes the set of mixed-integer linear service and system constraints that are common to both models and are, respectively, related to the routing (section 3.3.1), power scheduling (section 3.3.4), and output power (section 3.3.5) of MPSs, the routing (section 3.3.2) and operational service (section 3.3.3) constraints of RCs, the power balance (section 3.3.6), and power flow (section 3.3.7) constraints in the DS. In Appendix B, we list the notations for sets (Table B.1), parameters (Table B.2), and decision variables (Table B.3) used in the mathematical formulations of the two **MSO** models proposed in this study. As shown in Table B.3, a wide variety of decisions must be taken to achieve the pursued objectives, featuring the complexity of the decision making for DS restoration.

3.2.1. Mobile Service Optimization for Minimal Restoration Time (MSO-MRT). The model **MSO-MRT** minimizes the time needed for full restoration across the entire DS network. The term *full restoration* refers to the 100% restoration of the electric service—which has experienced an outage following an HILP incident, that is, the return of the system electric

supply demand balance to its normal pre-event condition (Arif et al. 2018, Chen et al. 2018, Dehghanian 2017, Lei et al. 2019b). The electricity supply outages across the network are realized as the network connectivity is disrupted following the HILP incident. Full restoration can hence be achieved either (i) when all damaged branches and equipment failures in the system are fixed and cleared via extensive maintenance—that is the original network connectivity is re-established, or (ii) when additional resilience delivery measures and services are utilized locally. In this study, the coordination of RC and MPS resources is considered as a resilience-delivery mechanism, which results in a full electric service restoration earlier. The MPSs temporarily supply the load points in the system with their energy needs, facilitating a faster restoration. That is, all load points can be served (full restoration is achieved) while the system's original connectivity is not yet established. Problem **MSO-MRT** is an MILP problem formulated as follows:

$$\mathbf{MSO-MRT}: \min \sum_{t=\tau}^{|\mathbf{T}|} t\mathbf{w}_t \tag{1a}$$

$$\text{s.to}\, \mathbf{w}_t \le \boldsymbol{\theta}_{i,t} \quad i \in \mathbf{B^o},\, t = \tau,\, \ldots,\, |\mathbf{T}| \tag{1b}$$

$$\boldsymbol{\phi}^+_{i,t} + \boldsymbol{\phi}^-_{i,t} \le (1 - \boldsymbol{\theta}_{i,t})(O^+_i + O^-_i) \quad i \in \mathbf{B^o},\, t = \tau,\, \ldots,\, |\mathbf{T}| \tag{1c}$$

$$\sum_{t=\tau}^{|\mathbf{T}|} \mathbf{w}_t \ge 1 \tag{1d}$$

$$\mathbf{w}, \boldsymbol{\theta} \in \{0, 1\} \tag{1e}$$

$$\mathbf{x} \in \mathfrak{F} \tag{1f}$$

The linear objective function (1a) minimizes the number of time periods needed to achieve full restoration, through effective management of MPSs and RCs, in the DS network. The binary variable $\mathbf{w}_t$ indicates the *earliest* time period t at which the electric service is fully restored, that is, all electricity outages in the network are fixed ($\mathbf{w}_t = 1$), or ($\mathbf{w}_t = 0$) otherwise. This condition is ensured through the introduction of the logical constraints (1b) and (1c). Recall that the electric power could be fully restored by coordinating the existing MPS/RC resources (i.e., the system is electrically restored), while there might be some damaged branches in the DS remained yet to be repaired by the RCs (i.e., the system is not structurally restored). To that end, $\mathbf{w}_t$ gets the value 1 only once, which is the first time at which the system has reached its full electrical restoration via effective utilization of MPSs/RCs—see constraint (1d) and objective function (1a). $\mathbf{w}_t = 1$ would become 0 later on while all arc failures have not been yet repaired but the DS has been electrically restored. Constraint (1c) checks whether the outage at node i is fixed ($\boldsymbol{\theta}_{i,t} = 1$) or not ($\boldsymbol{\theta}_{i,t} = 0$) at time t and depends on whether the amount of real $\boldsymbol{\phi}^+_{i,t}$ and reactive $\boldsymbol{\phi}^-_{i,t}$ power outage at this node is null at time t. Note that *reactive power* is different from *active power* which is actually supplied to the load points. In a power system, real power or active power is actually required or consumed by customers. Reactive power is just the portion of the electric power that helps establish the flow of electricity, maintain the voltage requirements across the power grid, and sustain the electric and magnetic fields required by alternating current equipment (Glover et al. 2012). The maximum real and reactive power demands at node i are denoted by O^+_i and O^-_i. Constraint (1b) ensures that service in the entire DS is fully restored at time t only if service is restored at each outage node at t. Constraint (1d) ensures that all outages are fixed within the allocated time. Omitting constraint (1d) would lead to an optimal value of 0 in which the power outages are not fixed, which is obviously not acceptable. Constraint (1e) defines the binary nature of $\mathbf{w}$ and $\boldsymbol{\theta}$. Constraint (1f) reflects that the aggregated vector $\mathbf{x}$ of decision variables must belong to the mixed-integer linear feasible set $\mathfrak{F}$ defined by the service and system constraints that are common to both models and presented in sections 3.3.1–3.3.7. The vector $\mathbf{x}$ is the concatenation of all the decision variables (see Table B.3 in Appendix B) and is used to ease the notations.

3.2.2. Mobile Service Optimization for Minimal Loss of Power (MSO-MPL). The MILP problem **MSO-MPL** minimizes the amount of power outage during the restoration process:

$$\mathbf{MSO-MPL}: \min \sum_{i \in \mathbf{B}} \sum_{t \in \mathbf{T}} \boldsymbol{\phi}^+_{i,t} \tag{2a}$$

$$\text{s.to}\ \mathbf{x} \in \mathfrak{F} \tag{2b}$$

The objective function (2a) minimizes the total amount of lost power during the restoration process, where $\boldsymbol{\phi}^+_{i,t}$ denotes the real power outage at node i at time t. In the DS, an MPS can supply power only to those DS nodes which are equipped with specific electrical facilities. We hereafter call such point-of-connection nodes *candidate nodes* (Yang et al. 2020). Constraint (2b) requires all general service and system constraints to be satisfied.

3.3. Common Service and System Constraints

This subsection presents the system and service constraints that are common to and enforced in both **MSO-MRT** and **MSO-MPL** models presented in this study. These constraints (routing of MPSs and RCs, power restoration, service of RCs, power schedules of MPSs, output power of MPSs, DS power balance, and

DS power flow) define a mixed-integer linear feasible set denoted by $\mathfrak{F}$ which must be satisfied by both **MSO-MRT** and **MSO-MPL** models, and are described in the next sections.

3.3.1. Routing Constraints for Mobile Power Sources. The MPSs' routing constraints define the integer linear feasible set:

$$\mathcal{F}^L_{R,MPS} := \{(\boldsymbol{\beta}, \boldsymbol{\gamma} \in \{0,1\} : (4a) - (4e))\} \tag{3}$$

with binary decision variables $\boldsymbol{\gamma}$ and $\boldsymbol{\beta}$, and constraints:

$$\mathcal{F}^L_{R,MPS} := \begin{cases} \sum_{a \in \mathbf{D}} \boldsymbol{\beta}_{a,m,t} \le 1 & m \in \mathbf{M}, t \in \mathbf{T} \quad (4a) \\ \boldsymbol{\beta}_{b,m,t+k} \le 1 - \boldsymbol{\beta}_{a,m,t} & m \in \mathbf{M}, a, b \in \mathbf{D^d}, k \le T^m_{a,b}, t \le |\mathbf{T}| - k \quad (4b) \\ \boldsymbol{\beta}_{1,m,1} = 1 & m \in \mathbf{M} \quad (4c) \\ \sum_{m \in \mathbf{M}} \boldsymbol{\beta}_{a,m,t} \le M_a & a \in \mathbf{D^d}, t \in \mathbf{T} \quad (4d) \\ \boldsymbol{\beta}_{a,m,t} \ge W_{a,i} \cdot \boldsymbol{\gamma}_{i,m,t} & m \in \mathbf{M}, a \in \mathbf{D^d}, i \in \mathbf{B^m}, t \in \mathbf{T} \quad (4e) \end{cases}$$

Each MPS m can be at one TS node a at any time period t as required by (4a). The routing of MPSs is defined by constraint (4b). The binary variable $\boldsymbol{\beta}_{a,m,t}$ indicates whether MPS m is at TS node a at time period t ($\boldsymbol{\beta}_{a,m,t} = 1$) or not ($\boldsymbol{\beta}_{a,m,t} = 0$). For example, if MPS m is at TS node a at time $t = 1$ (i.e., $\boldsymbol{\beta}_{a,m,1} = 1$) and needs three time periods to travel through the path a–b and arrive at node b (i.e., $T^m_{a,b} = 3$), then MPS m will arrive at node b at $t = 4$ (i.e., $\boldsymbol{\beta}_{b,m,4} = 1$), which implies $\boldsymbol{\beta}_{b,m,2} = 0$ and $\boldsymbol{\beta}_{b,m,3} = 0$. Constraint (4c) specifies the initial location of the MPSs which are all pre-positioned at the emergency center, that is, TS node 1. Constraint (4d) ensures that the total number of MPSs located at TS node a at any time period does not exceed the maximum number of vehicles that node a can host.

The interconnection of the TS and DS must be considered to schedule the MPSs and is modeled with (4e). The notation $\mathbf{B^m}$ in (4e) is the set of *candidate nodes*, which are DS nodes equipped with specific electrical facilities that allow MPSs to be connected to the DS. There exists a correspondence between the DS candidate nodes and the TS nodes, hereafter called coupling points/nodes (Wei et al. 2019). The binary parameter $W_{a,i}$ defines the *coupling nodes* that tie the DS and the TS, and is equal to 1 if TS node a and DS candidate node i are coupling nodes, and is 0 otherwise. The binary variable $\boldsymbol{\gamma}_{i,m,t}$ indicates whether MPS m is connected to DS node i at time t ($\boldsymbol{\gamma}_{i,m,t} = 1$) or not ($\boldsymbol{\gamma}_{i,m,t} = 0$). A simple example for the interconnection of the TS and DS is presented in Figure 6. One can see that there exist two coupling nodes between the TS and DS (i.e., $T3$–$D2$, $T5$–$D5$); thereby we have $W_{3,2} = W_{5,5} = 1$ and $W_{a,i} = 0$ for the remaining node pairs. Integrating this with constraint (4e), the correspondence between the TS and DS is captured by the two constraints $\boldsymbol{\beta}_{3,m,t} \ge \boldsymbol{\gamma}_{2,m,t}$ and $\boldsymbol{\beta}_{5,m,t} \ge \boldsymbol{\gamma}_{5,m,t}$. Constraint (4e) ensures that the DS candidate node i can be served by MPS m only if it reaches the coupling node a at time t.

3.3.2. Routing Constraints for Repair Crews. The RCs' routing constraints define the integer linear feasible set:

$$\mathcal{F}^L_{R,RC} := \{(\mathbf{y}, \mathbf{z} \in \{0,1\} : (6a) - (6e))\} \tag{5}$$

with binary decision variables $\mathbf{y}$ and $\mathbf{z}$, and constraints:

$$\mathcal{F}^L_{R,RC} := \begin{cases} \sum_{a \in \mathbf{D}} \mathbf{y}_{a,c,t} \le 1 & c \in \mathbf{C}, t \in \mathbf{T} \quad (6a) \\ \mathbf{y}_{b,c,t+k} \le 1 - \mathbf{y}_{a,c,t} & c \in \mathbf{C}, a, b \in \mathbf{D^d}, k \le T^c_{a,b}, t \le |\mathbf{T}| - k \quad (6b) \\ \mathbf{y}_{1,c,1} = 1 & c \in \mathbf{C} \quad (6c) \\ \sum_{c \in \mathbf{C}} \mathbf{y}_{a,c,t} \le M_a & a \in \mathbf{D^d}, t \in \mathbf{T} \quad (6d) \\ \mathbf{y}_{a,c,t} \ge E_{a,l} \cdot \mathbf{z}_{l,c,t} & c \in \mathbf{C}, a \in \mathbf{D^d}, l \in \mathbf{L^d}, t \in \mathbf{T} \quad (6e) \end{cases}$$

Figure 6 Mapping Example Between the TS and DS [Color figure can be viewed at wileyonlinelibrary.com]

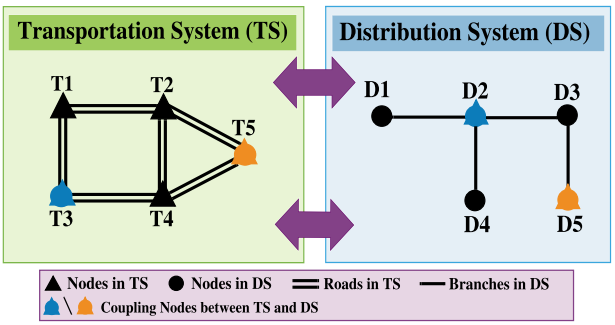

The routing and scheduling constraints (6a)–(6e) for RCs are similar to constraints (4a)–(4e) for MPSs. Constraint (6a) ensures that an RC can only be at one TS node a at any time period t. The routing of the RCs in the TS is defined with constraint (6b). The binary variable $\mathbf{y}_{a,c,t}$ defines whether RC c is located at TS node a at time t. Constraint (6c) states that all RCs are located at TS node 1 at the initial period of the restoration process. Constraint (6d) ensures that the total number of RCs located at TS node a at time period t does not exceed the vehicles' capacity of node a. Constraint (6e), which is the counterpart of constraint (4e) for MPSs, defines the mapping between the TS and the DS and its impact on the RCs' schedules. Different from MPSs which supply power to DS candidate nodes, RCs repair damaged branches. The binary parameter $E_{a,l}$ defines the correspondence between TS node a and the repair zone around the damaged branch l in the DS. The binary variable $\mathbf{z}_{l,c,t}$ indicates whether RC c is at branch l at time t. Constraint (6e) stipulates that a damaged branch can be repaired by RC c only if it reaches the coupling node a in the TS at time t.

3.3.3. Service Constraints for Repair Crews.

The RCs' service constraints define the integer linear feasible set:

$$\mathcal{F}^{L}_{S,RC} := \{(\mathbf{z}, \boldsymbol{\mu} \in \{0,1\} : (8a) - (8d))\} \tag{7}$$

with binary decision variables $\mathbf{z}$ and $\boldsymbol{\mu}$, and constraints:

$$\mathcal{F}^{L}_{S,RC} := \begin{cases} \mu_{l,t} \le \frac{\sum_{k=1}^{t} \mathbf{z}_{l,c,k}}{T_l} & c \in \mathbf{C}, l \in \mathbf{L}^{\mathbf{d}}, t = T_l, \ldots, |\mathbf{T}| \quad (8a) \\ \mu_{l,t} \ge \frac{\sum_{k=1}^{t} \mathbf{z}_{l,c,k}}{T_l} - \frac{T_l - 1}{T_l} & c \in \mathbf{C}, l \in \mathbf{L}^{\mathbf{d}}, t = T_l, \ldots, |\mathbf{T}| \quad (8b) \\ \mu_{l,t} = 0 & l \in \mathbf{L}^{\mathbf{d}}, t = 1, \ldots, T_l - 1 \quad (8c) \\ \mu_{l,t} = 1 & l \in \mathbf{L} \setminus \mathbf{L}^{\mathbf{d}}, t \in \mathbf{T} \quad (8d) \end{cases}$$

Constraints (8a) and (8b) enforce conditions on the status of a damaged branch l and the RC assignments. The binary variable $\boldsymbol{\mu}_{l,t}$ defines the status of branch l at time t (i.e., l is operational if $\boldsymbol{\mu}_{l,t} = 1$). Constraint (8a) imposes $\boldsymbol{\mu}_{l,t} = 0$ if an RC has not devoted the minimal time T_l needed to repair the damaged branch l. On the other hand, the right side of (8b) is strictly positive only if an RC has spent T_l periods to repair branch l, which in turn forces $\boldsymbol{\mu}_{l,t} = 1$. Constraint (8c) indicates that a damaged branch l is disconnected from the DS until $T_l - 1$, since T_l is the earliest time at which branch l can possibly be repaired. Constraint (8d) states that each undamaged branch is connected and online during the entire restoration process.

3.3.4. Power Scheduling Constraints for Mobile Power Sources.

We recall that two types of distinct MPSs technologies, that is, MEGs and MESSs, are considered for DS restoration following an HILP incident. Their differences and impacts on the restoration process are reflected by the specifics of their respective power scheduling constraints presented in this subsection. The MPSs' power scheduling constraints define the mixed-integer linear feasible set:

$$\mathcal{F}^{L}_{M,PS} := \{(\boldsymbol{\lambda}^{+}, \boldsymbol{\lambda}^{-}, \boldsymbol{\pi}^{+}, \boldsymbol{\pi}^{-}, \mathbf{s}, \boldsymbol{\gamma}, \boldsymbol{\delta}^{+}, \boldsymbol{\delta}^{-}) \in \mathbb{R}_{+} \times \{0,1\} : (10a) - (10i))\} \tag{9}$$

with nonnegative continuous variables $(\boldsymbol{\lambda}^{+}, \boldsymbol{\lambda}^{-}, \boldsymbol{\pi}^{+}, \boldsymbol{\pi}^{-}, \mathbf{s})$, binary variables $(\boldsymbol{\gamma}, \boldsymbol{\delta}^{+}, \boldsymbol{\delta}^{-})$, and constraints:

$$\mathcal{F}^{L}_{M,PS} := \begin{cases} \lambda^{+}_{i,m,t} \le \gamma_{i,m,t} \cdot P_m & i \in \mathbf{B}^{\mathbf{m}}, m \in \mathbf{M}^{\mathbf{g}}, t \in \mathbf{T} \quad (10a) \\ \lambda^{-}_{i,m,t} \le \gamma_{i,m,t} \cdot Q_m & i \in \mathbf{B}^{\mathbf{m}}, m \in \mathbf{M}^{\mathbf{g}}, t \in \mathbf{T} \quad (10b) \\ \epsilon_1 \cdot \gamma_{i,m,t} \le \lambda^{+}_{i,m,t} + \lambda^{-}_{i,m,t} & i \in \mathbf{B}^{\mathbf{m}}, m \in \mathbf{M}^{\mathbf{g}}, t \in \mathbf{T} \quad (10c) \\ \pi^{+}_{i,m,t} \le \delta^{+}_{i,m,t} \cdot J^{+}_{m} & i \in \mathbf{B}^{\mathbf{m}}, m \in \mathbf{M}^{\mathbf{s}}, t \in \mathbf{T} \quad (10d) \\ \pi^{-}_{i,m,t} \le \delta^{-}_{i,m,t} \cdot J^{-}_{m} & i \in \mathbf{B}^{\mathbf{m}}, m \in \mathbf{M}^{\mathbf{s}}, t \in \mathbf{T} \quad (10e) \\ \delta^{-}_{i,m,t} + \delta^{+}_{i,m,t} \le \gamma_{i,m,t} & i \in \mathbf{B}^{\mathbf{m}}, m \in \mathbf{M}^{\mathbf{s}}, t \in \mathbf{T} \quad (10f) \\ \epsilon_2 \cdot \gamma_{i,m,t} \le \pi^{+}_{i,m,t} + \pi^{-}_{i,m,t} & i \in \mathbf{B}^{\mathbf{m}}, m \in \mathbf{M}^{\mathbf{s}}, t \in \mathbf{T} \quad (10g) \\ \mathbf{s}_{m,t+1} - \mathbf{s}_{m,t} = \left(\sum_{i \in \mathbf{B}^{\mathbf{m}}} \pi^{-}_{i,m,t} \cdot Z^{-}_{m} - \frac{\sum_{i \in \mathbf{B}^{\mathbf{m}}} \pi^{+}_{i,m,t}}{Z^{+}_{m}} \right) & m \in \mathbf{M}^{\mathbf{s}}, t \le |\mathbf{T}| - 1 \quad (10h) \\ \underline{S}_m \le \mathbf{s}_{m,t} \le \overline{S}_m & m \in \mathbf{M}^{\mathbf{s}}, t \in \mathbf{T} \quad (10i) \\ \mathbf{s}_{m,1} = \overline{\mathbf{S}}_m & m \in \mathbf{M}^{\mathbf{s}} \quad (10j) \end{cases}$$

The variables $\boldsymbol{\lambda}^{+}_{i,m,t}$ and $\boldsymbol{\lambda}^{-}_{i,m,t}$ respectively denote the maximum real and reactive power output of MEG m. Constraints (10a) and (10b) represent the range of real and reactive output power of MEG m. The output power of MEGs is upper-bounded by their real (P_m) and reactive (Q_m) power capacities. Since ϵ_1 is the minimum production level of real and reactive power under which it is not efficient to connect an MEG to a candidate node, (10c) ensures that any MEG produces enough real and reactive power when connected to a candidate node. The output power of the MESSs is modeled with constraints (10d)–(10g). The binary variable $\boldsymbol{\delta}^{-}_{i,m,t}$ (resp., $\boldsymbol{\delta}^{+}_{i,m,t}$) takes value 1 if MESS m is charging (resp., discharging) at node i at time t, and is equal to 0 otherwise. Constraints (10d) and (10e) restrict the MESSs' charging and discharging power capacities, respectively. When MPS m is in a charging

state at time t ($\boldsymbol{\delta}^{-}_{i,m,t}=1$), the power needed for its charging power $\boldsymbol{\pi}^{-}_{i,m,t}$ at time t cannot exceed the upper bound J^{-}_{m}. Similarly, if in a discharging state at time t ($\boldsymbol{\delta}^{+}_{i,m,t}=1$), the delivered power $\boldsymbol{\pi}^{+}_{i,m,t}$ by MESS m to the candidate node i at t cannot exceed the bound J^{+}_{m}. Constraint (10f) ensures that MESS m can neither charge nor discharge at candidate node i at time t if it is not connected ($\boldsymbol{\gamma}_{i,m,t}=0$) to candidate node i at t and expresses that the charging and discharging states are mutually exclusive: any MESS m connected to a candidate node i cannot be in charging and discharging state at the same time. Constraint (10g) guarantees that an MESS m produces a sufficient amount (i.e., $\geq \epsilon_2$) of charging and discharging power if connected to a DS candidate node i at any time t. Constraint (10h) represents the variations in the state of charge (SOC) of MESS m over time, which is determined by MESSs' charging and discharging behaviors. The parameters Z^{-}_{m} and Z^{+}_{m} are the charging and discharging efficiency of MESS m. The SOC of the MESSs are lower- and upper-bounded at each time period by (10i). Constraint (10j) ensures that the SOC of the MESS m at the initial time $t=1$ is set to its maximum value.

3.3.5. Output Power Constraints for Mobile Power Sources. The output power constraints for MPSs define the linear set:

$$\mathcal{F}^{L}_{M,O} := \{(\mathbf{p},\mathbf{q},\boldsymbol{\lambda}^{+},\boldsymbol{\lambda}^{-}) \in \mathbb{R}\times\mathbb{R}_{+} : (12a)-(12c))\} \tag{11}$$

with continuous variables $\mathbf{p}$ (sign-unrestricted), $\mathbf{q}$, $\boldsymbol{\lambda}^{+}$, $\boldsymbol{\lambda}^{-}$ (nonnegative), and constraints:

$$\mathcal{F}^{L}_{M,O} := \begin{cases} \mathbf{p}_{i,t} = \sum\limits_{m\in\mathbf{M^g}} \lambda^{+}_{i,m,t} + \sum\limits_{m\in\mathbf{M^s}} (\boldsymbol{\pi}^{+}_{i,m,t} - \boldsymbol{\pi}^{-}_{i,m,t}) & i\in\mathbf{B^m}, t\in\mathbf{T} \quad (12a)\\ \mathbf{q}_{i,t} = \sum\limits_{m\in\mathbf{M^g}} \lambda^{-}_{i,m,t} & i\in\mathbf{B^m}, t\in\mathbf{T} \quad (12b)\\ \mathbf{p}_{i,t} = \mathbf{q}_{i,t} = 0 & i\in\mathbf{B}\setminus\mathbf{B^m}, t\in\mathbf{T} \quad (12c) \end{cases}$$

The real and reactive power load supplied at any time t at node i is equal to the sum of the real and reactive power output of each MPS stationed at node i at time t. Constraint (12a) and (12b) determine the real or reactive power injection or extraction at a candidate node i served by MPSs. The value of $\mathbf{p}_{i,t}$ can be either positive or negative. If $\mathbf{p}_{i,t}$ is negative (resp., positive) at time t, the net real power at candidate node i at time t will be negative (resp., positive) reflecting a net charging (resp., discharging) state for the connected MPSs. Constraint (12c) ensures that $\mathbf{p}_{i,t}$ and $\mathbf{q}_{i,t}$ are zero if node i is not a candidate node.

3.3.6. Power Balance Constraints. The DS' power balance constraints define the mixed-integer linear feasible set:

$$\mathcal{F}^{L}_{DS,PB} := \{(\mathbf{p},\mathbf{q},\mathbf{h}^{+},\mathbf{h}^{-},\boldsymbol{\phi}^{+},\boldsymbol{\phi}^{-},\boldsymbol{\psi}^{+},\boldsymbol{\psi}^{-},\boldsymbol{\mu}) \in \mathbb{R}\times\mathbb{R}_{+}\times\{0,1\} : (14a)-(14l))\} \tag{13}$$

with continuous variables $\mathbf{p}$ (sign-unrestricted), $\mathbf{q}$, $\mathbf{h}^{+}$, $\mathbf{h}^{-}$, $\boldsymbol{\phi}^{-}$, $\boldsymbol{\phi}^{+}$, $\boldsymbol{\psi}^{+}$, and $\boldsymbol{\psi}^{-}$ (nonnegative), binary variables $\boldsymbol{\mu}$, and constraints:

$$\mathcal{F}^{L}_{DS,PB} := \begin{cases} \sum\limits_{l(i,j)\in\mathbf{L}} \mathbf{h}^{+}_{l,t} + (O^{+}_{i} - \boldsymbol{\phi}^{+}_{i,t}) = \sum\limits_{l(j,i)\in\mathbf{L}} \mathbf{h}^{+}_{l,t} + \boldsymbol{\psi}^{+}_{i,t} + \mathbf{p}_{i,t} & i\in\mathbf{B^o}, t\in\mathbf{T} \quad (14a)\\ \sum\limits_{l(i,j)\in\mathbf{L}} \mathbf{h}^{-}_{l,t} + (O^{-}_{i} - \boldsymbol{\phi}^{-}_{i,t}) = \sum\limits_{l(j,i)\in\mathbf{L}} \mathbf{h}^{-}_{l,t} + \boldsymbol{\psi}^{-}_{i,t} + \mathbf{q}_{i,t} & i\in\mathbf{B^o}, t\in\mathbf{T} \quad (14b)\\ \sum\limits_{l(i,j)\in\mathbf{L}} \mathbf{h}^{+}_{l,t} + O^{+}_{i} = \sum\limits_{l(j,i)\in\mathbf{L}} \mathbf{h}^{+}_{l,t} + \boldsymbol{\psi}^{+}_{i,t} + \mathbf{p}_{i,t} & i\in\mathbf{B}\setminus\mathbf{B^o}, t\in\mathbf{T} \quad (14c)\\ \sum\limits_{l(i,j)\in\mathbf{L}} \mathbf{h}^{-}_{l,t} + O^{-}_{i} = \sum\limits_{l(j,i)\in\mathbf{L}} \mathbf{h}^{-}_{l,t} + \boldsymbol{\psi}^{-}_{i,t} + \mathbf{q}_{i,t} & i\in\mathbf{B}\setminus\mathbf{B^o}, t\in\mathbf{T} \quad (14d)\\ 0 \leq \boldsymbol{\phi}^{+}_{i,t} \leq O^{+}_{i} & i\in\mathbf{B^o}, t\in\mathbf{T} \quad (14e)\\ \boldsymbol{\phi}^{-}_{i,t} \leq \boldsymbol{\phi}^{+}_{i,t}\cdot(O^{-}_{i}/O^{+}_{i}) & i\in\mathbf{B^o}, t\in\mathbf{T} \quad (14f)\\ -\boldsymbol{\mu}_{l,t}\cdot H^{+}_{l} \leq \mathbf{h}^{+}_{l,t} \leq \boldsymbol{\mu}_{l,t}\cdot H^{+}_{l} & l\in\mathbf{L}, t\in\mathbf{T} \quad (14g)\\ -\boldsymbol{\mu}_{l,t}\cdot H^{-}_{l} \leq \mathbf{h}^{-}_{l,t} \leq \boldsymbol{\mu}_{l,t}\cdot H^{-}_{l} & l\in\mathbf{L}, t\in\mathbf{T} \quad (14h)\\ \underline{F}^{+} \leq \boldsymbol{\psi}^{+}_{1,t} \leq \overline{F}^{+} & t\in\mathbf{T} \quad (14i)\\ \underline{F}^{-} \leq \boldsymbol{\psi}^{-}_{1,t} \leq \overline{F}^{-} & t\in\mathbf{T} \quad (14j)\\ \boldsymbol{\psi}^{+}_{i,t} = \boldsymbol{\psi}^{-}_{i,t} = 0 & i=2,\ldots,|\mathbf{B}|, t\in\mathbf{T} \quad (14k)\\ \boldsymbol{\phi}^{+}_{i,t+1} \leq \boldsymbol{\phi}^{+}_{i,t} & i\in\mathbf{B^o}, t\leq|\mathbf{T}|-1 \quad (14l)\\ \boldsymbol{\phi}^{-}_{i,t+1} \leq \boldsymbol{\phi}^{-}_{i,t} & i\in\mathbf{B^o}, t\leq|\mathbf{T}|-1 \quad (14m) \end{cases}$$

Constraints (14a) and (14b) describe the real and reactive power balance conditions at outage nodes, respectively, and enforce Kirchhoff's first law which stipulates that the total incoming power flow must be equal to the total outgoing power flow. Constraints (14c) and (14d) do the same for the nodes that do not undergo any outage. Constraint (14e) ensures that the amount of real power outage at node i does not exceed the maximum demand at node i. In a DS, the demand power factor is defined as the ratio of supplied real power to the demand and apparent power flowing through the circuit (Glover et al. 2012). The demand power factor is fixed and equal to (O_i^-/O_i^+). The relationship between the restored real and reactive load is defined by (14f). The real and reactive power flows in online branches are limited by their real and reactive power capacities defined in (14g) and (14h). The substation (commonly the first node in the DS) is connected to the upstream (transmission) network and transfers the electric power to the DS. The bounds on the generation of real and reactive power at the substation (DS node 1) are set by (14i) and (14j). Constraint (14k) enforces that there is no real and reactive power generation at other nodes than the substation node. Constraints (14l) and (14m), respectively, ensure that the real and reactive power outages at any node i decrease as the restoration process progresses.

3.3.7. Power Flow Constraints. The DS' power flow constraints define the mixed-integer linear feasible set:

$$\mathcal{F}^L_{DS,PF} := \{(\mathbf{v}, \mathbf{h}^+, \mathbf{h}^-, \boldsymbol{\mu}) \in \mathbb{R}_+ \times \{0,1\} : (16a) - (16c))\} \tag{15}$$

with nonnegative continuous variables $\mathbf{v}$, $\mathbf{h}^+$, and $\mathbf{h}^-$, binary variable $\boldsymbol{\mu}$, and constraints:

$$\mathcal{F}^L_{DS,PF} := \begin{cases} \mathbf{v}_{i,t} - \mathbf{v}_{j,t} \le (1-\boldsymbol{\mu}_{l,t}) \cdot U + 2 \cdot (R_l \mathbf{h}^+_{l,t} + X_l \mathbf{h}^-_{l,t}) & i,j \in \mathbf{B}, l \in \mathbf{L}, t \in \mathbf{T} \quad (16a) \\ \mathbf{v}_{i,t} - \mathbf{v}_{j,t} \ge (\boldsymbol{\mu}_{l,t}-1) \cdot U + 2 \cdot (R_l \mathbf{h}^+_{l,t} + X_l \mathbf{h}^-_{l,t}) & i,j \in \mathbf{B}, l \in \mathbf{L}, t \in \mathbf{T} \quad (16b) \\ \underline{V}_i \le \mathbf{v}_{i,t} \le \overline{V}_i & i \in \mathbf{B}, t \in \mathbf{T} \quad (16c) \end{cases}$$

Constraints (16a) and (16b) represent the power flow equation considering the status of the DS branches, where the terms $(1-\boldsymbol{\mu}_{l,t})U$ and $(\boldsymbol{\mu}_{l,t}-1)U$ ensure that the power flow condition is satisfied if branch l is connected and online. The parameter U is the maximum value for the difference in squared voltage magnitude in DS nodes. If the branch l between nodes i and j is connected ($\boldsymbol{\mu}_{l,t}=1$), the terms $(1-\boldsymbol{\mu}_{l,t})U$ and $(\boldsymbol{\mu}_{l,t}-1)U$ vanish in (16a) and (16b). If the branch is disconnected ($\boldsymbol{\mu}_{l,t}=0$), the second term in the right side of (16a) and (16b) is 0 due to (14g) and (14h). Constraint (16c) defines the lower and upper bounds on the squared voltage magnitude $\mathbf{v}_{i,t}$.

3.4. Model Strengthening with Valid Inequalities

The two proposed **MSO-MRT** and **MSO-MPL** models are complex MILPs and computationally intensive to solve even with state-of-the-art optimization solvers, such as Cplex and Gurobi. The models quickly become very large, even for moderate-size networks, due in particular to the interdependence and mapping of the DS and the TS networks. While the primary objective of this study is not computational nor algorithmic, it is yet important to be able to efficiently solve the above two models for practice-size instances. *Model strengthening* here must be understood in terms of the branch-and-bound algorithmic process used to solve MILP problems and in particular to the continuous relaxation of the MILP problem and its feasible area. We strengthen the model by deriving valid inequalities in order to obtain a tighter formulation whose continuous relaxation is *closer* to the true original problem and to speed up the solution process. The valid inequalities do not eliminate any integer feasible solution (thereby keeping the feasible area of the MILP problem unchanged) but do eliminate some fractional solutions that would have been otherwise feasible and included in the feasible area of the continuous relaxation problem. The following constraints are valid inequalities for the two proposed models **MSO-MRT** and **MSO-MPL**:

$$\sum_{c \in \mathbf{C}} \mathbf{z}_{l,c,t} \le 1 \; l \in \mathbf{L^d}, t \in \mathbf{T} \tag{17a}$$

$$\sum_{c \in \mathbf{C}} \sum_{t \in \mathbf{T}} \mathbf{z}_{l,c,t} = T_l \; l \in \mathbf{L^d} \tag{17b}$$

$$\boldsymbol{\mu}_{l,t} \le \boldsymbol{\mu}_{l,t+1} \; l \in \mathbf{L^d}, t \le |\mathbf{T}| - 1 \tag{17c}$$

$$\boldsymbol{\theta}_{i,t} \le \boldsymbol{\theta}_{i,t+1} \; i \in \mathbf{B^o}, t = \tau, \ldots, |\mathbf{T}| - 1 \tag{17d}$$

$$\gamma_{i,m,t+1} \le |\mathbf{L_i^d}| - \sum_{l \in \mathbf{L_i^d}} \mu_{l,t} \; m \in \mathbf{M^g}, i \in \mathbf{B^o}, t \le |\mathbf{T}| - 1 \quad (17e)$$

$$\gamma_{i,m,t+1} \le |\mathbf{L^d}| - \sum_{l \in \mathbf{L^d}} \mu_{l,t} \; m \in \mathbf{M^s}, i \in \mathbf{B^o}, t \le |\mathbf{T}| - 1 \quad (17f)$$

$$\mathbf{z}_{l,c,t+1} \le 1 - \mu_{l,t} \; c \in \mathbf{C}, l \in \mathbf{L^d}, t \le |\mathbf{T}| - 1 \quad (17g)$$

$$\delta^+_{i,m,t+1} \le |\mathbf{L_i^d}| - \sum_{l \in \mathbf{L_i^d}} \mu_{l,t} \; m \in \mathbf{M^s}, i \in \mathbf{B^m}, t \le |\mathbf{T}| - 1 \quad (17h)$$

$$\delta^-_{i,m,t+1} \le |\mathbf{L^d}| - \sum_{l \in \mathbf{L^d}} \mu_{l,t} \; m \in \mathbf{M^s}, i \in \mathbf{B^m}, t \le |\mathbf{T}| - 1 \quad (17i)$$

$$\varepsilon_3(1 - \theta_{i,t}) \le \phi^+_{\mathbf{i,t}} + \phi^-_{\mathbf{i,t}} \; i \in \mathbf{B^m}, t \in T \quad (17j)$$

$$1 - \theta_{i,t+1} \le |\mathbf{L_i^d}| - \sum_{l \in \mathbf{L_i^d}} \mu_{l,t} \; i \in \mathbf{B^m}, t \le |\mathbf{T}| - 1 \quad (17k)$$

$$\phi^+_{i,t+1} \le (|\mathbf{L_i^d}| - \sum_{l \in \mathbf{L_i^d}} \mu_{l,t}) O_i^+ \; i \in \mathbf{B^o}, t \le |\mathbf{T}| - 1 \quad (17l)$$

$$\phi^-_{i,t+1} \le (|\mathbf{L_i^d}| - \sum_{l \in \mathbf{L_i^d}} \mu_{l,t}) O_i^- \; i \in \mathbf{B^o}, t \le |\mathbf{T}| - 1 \quad (17m)$$

$$\pi^+_{i,m,t+1} \le (|\mathbf{L_i^d}| - \sum_{l \in \mathbf{L_i^d}} \mu_{l,t}) J_m^+ \; m \in \mathbf{M^s}, i \in \mathbf{B^m}, t \le |\mathbf{T}| - 1 \quad (17n)$$

$$\pi^-_{i,m,t+1} \le (|\mathbf{L^d}| - \sum_{l \in \mathbf{L^d}} \mu_{l,t}) J_m^- \; m \in \mathbf{M^s}, i \in \mathbf{B^m}, t \le |\mathbf{T}| - 1 \quad (17o)$$

$$\lambda^+_{i,m,t+1} \le (|\mathbf{L_i^d}| - \sum_{l \in \mathbf{L_i^d}} \mu_{l,t}) P_m \; m \in \mathbf{M^g}, i \in \mathbf{B^m}, t \le |\mathbf{T}| - 1 \quad (17p)$$

$$\lambda^-_{i,m,t+1} \le (|\mathbf{L_i^d}| - \sum_{l \in \mathbf{L_i^d}} \mu_{l,t}) Q_m \; m \in \mathbf{M^g}, i \in \mathbf{B^m}, t \le |\mathbf{T}| - 1 \quad (17q)$$

Constraint (17a) ensures that each damaged branch l is attended to by at most one RC at each period. Constraint (17b) hedges against RC wasting time and ensures that the RC assigned to mend the damaged branch l spends the minimal time T_l needed to fully repair that branch. The set of precedence constraints (17c) states that any damaged branch l stays online after having been repaired. Similarly, (17d) indicates that an outage node i remains online once service has been restored. Constraint (17e) ensures that MEGs are not connected to an outage node $i \in \mathbf{B^m}$ after the damaged branches that caused the outage at this node are fixed. This inequality is only enforced for MEGs since MESSs (the other type of MPSs) must be allowed to travel to a candidate node i – even after the service at node i is fully restored – to charge and hence enable them to subsequently travel to and restore power at the remaining outage nodes. This is not a possibility for MEGs which illustrates the operational differences between these two new MPS technologies. That is why the counterpart (17f) of (17e) for MESSs is less restrictive and prevents an MESS from connecting to any candidate node *i only once all* damaged branches in the network are mended and power is restored in the entire DS. Analogously, constraint (17g) ensures that RCs are not assigned to a damaged branch after its reparation. Constraint (17h) does not allow an MESS to be connected to a node i after the damaged branches that caused the outage at this node are fixed. Constraint (17i) allows MESSs to travel to candidate node i and charge their batteries even after all damaged branches are fixed and even if the service at node i is fully restored. Constraint (17k) fixes the value of the binary variable θ_i to one at all time periods once service has been restored at node i. Constraints (17l)–(17m) respectively ensure that the active and reactive power outages at node i will remain zero after the period t at which all damaged branches leading to the outage at node i are fixed. Constraint (17n) (resp., (17o)) ensures that MESSs stops delivering power to (resp., charging at) a candidate node i after the reparation of all the damaged branches that caused the outage at node i. Constraints (17p)–(17q) respectively force the active and reactive output power for MEGs to be null at any outage node i and at each period following the time at which all damaged branches causing the outage at that node are fixed.

4. Numerical Case Studies and Insights

Sections 4.1 and 4.3 describe the two different test systems to which the proposed analytics are applied. Sections 4.2 and 4.4 introduce the test scenarios employed to demonstrate the impacts of various factors on the service restoration process and the resilience objective. Such factors include (i) multi-branch damage scenarios in the DS, (ii) transportation sector disruptions during HILP events, (iii) repair time for branches in the DS, (iv) the choice of the service restoration strategy, (v) the variable availability of MPS resources, and (vi) more severe disruptions in both DS and TS.

4.1. Test System Description: Test System 1

We perform the computational experiments on a DS taking into account the TS conditions and restrictions during HILP events. The configuration of the test systems is illustrated in Figure 7, where the DS and TS networks are integrated through several coupling nodes defined in Table 1. The TS network is the Sioux Falls network and consists of 24 nodes and 76 arcs. The specific data (e.g., length of the arcs, speed limits

for vehicles traveling on each arc) are described in details by (Ukkusuri and Yushimito 2009). The DS is the IEEE 33-node test system which includes 1 substation, 32 branches, and 33 nodes serving a total electricity demand of 3,715 kW. The detailed information on each node and branch in the system is provided by Baran and Wu (1989). There are nine candidate nodes in the DS, to which an MPS can be connected for charging, power delivery (discharging), and service restoration. The TS (see Figure 7) owns nine coupling nodes mapped to nine DS candidate nodes and four coupling nodes mapped to four DS repair zones around specific branches. In this study, we consider employing MEGs with 400 kW/300 kVar capacity and MESSs with 300 kW/500 kWh capacity. All RCs and MPSs are pre-positioned at the emergency center (first node in the TS) when an HILP event occurs. The entire restoration time horizon in all the conducted tests is assumed to be 48 periods of five minutes (4 hours). The proposed MILP problems **MSO-MRT** and **MSO-MPL** are formulated with the AMPL algebraic modeling language and solved with the state-of-the-art optimization solver Gurobi 9.0.2.

4.2. Test Scenarios, Numerical Results, and Insights: Test System 1

We now verify the effectiveness of the presented schemes for DS restoration through the following six Test Cases (TCs), each with multiple scenarios:

1. **Test Case I (TCI)** presented in section 4.2.1 investigates the performance of the proposed models **MSO-MRT** and **MSO-MPL** under different branch damage scenarios in the DS, that is, different realizations of HILP events in DS. The transportation sector is here assumed fully reliable and not disrupted by the HILP event. The time needed for the RCs to repair each damaged branch is considered to be eight periods of five minutes (40 minutes). The following four scenarios (S) are investigated in **TCI** with both **MSO-MRT** and **MSO-MPL** models:
   - **(TCI–S1)** One-Branch Damage Scenario in the DS.
   - **(TCI–S2)** Two-Branch Damage Scenario in the DS.
   - **(TCI–S3)** Three-Branch Damage Scenario in the DS.
   - **(TCI–S4)** Four-Branch Damage Scenario in the DS.
2. **Test Case II (TCII)**, presented in section 4.2.2, investigates the performance of the proposed **MSO-MRT** and **MSO-MPL** models under different arc damage scenarios in the TS, that is, different realizations of the HILP event in both TS and DS. In order to highlight the role of the TS constraints in DS restoration and resilience, our analysis in **TCII** is based on a three-branch damage scenario in the DS (the same as that in **TCI-S3**), but under different arc damage scenarios in the TS. The time needed for the RCs to repair any damaged branch in the DS is

Table 1 Coupling Points in the Integrated TS and DS Networks in Test System 1

TS nodes	DS candidate nodes	TS nodes	DS repair zones
2	*n*32	8	*L*25(*n*6–*n*26)
4	*n*25	10	*L*22(*n*3–*n*23)
5	*n*28	13	*L*1(*n*1–*n*2)
14	*n*3	19	*L*8(*n*8–*n*9)
17	*n*12		
18	*n*18		
20	*n*9		
21	*n*20		
22	*n*6		

Figure 7 Configuration of the Integrated TS and DS Networks in Test System 1 [Color figure can be viewed at wileyonlinelibrary.com]

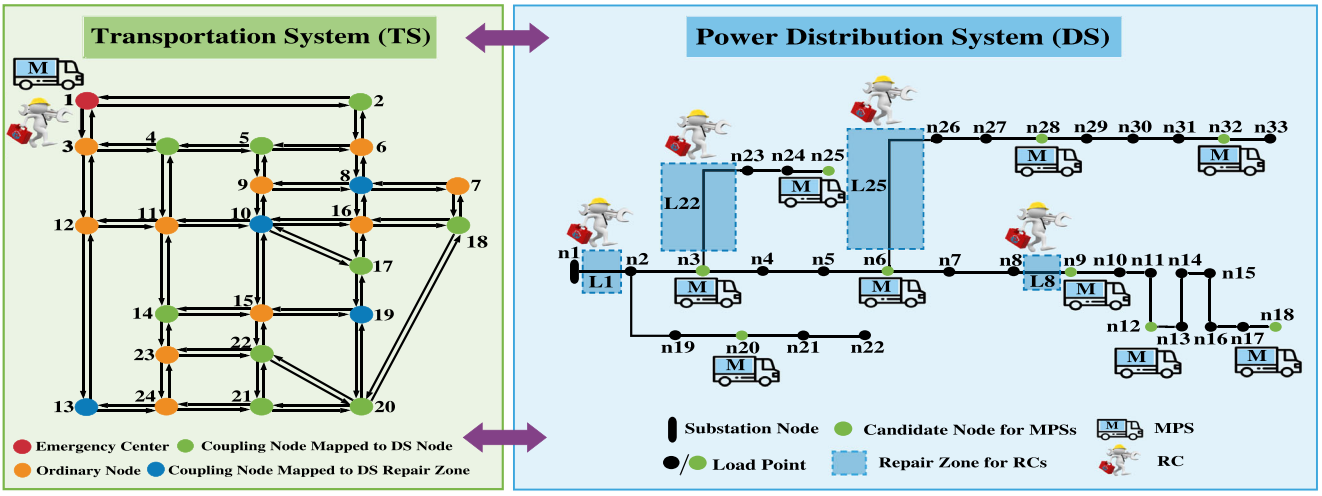

eight periods of five minutes while the damaged arcs in the TS are unavailable during the entire restoration process. This assumption is in line with the real-world practices as the reparation of the TS arcs (roads and streets) typically takes days, well beyond the 4-hour restoration time horizon considered here. The three scenarios (S) below are investigated in **TCII** for both **MSO-MRT** and **MSO-MPL** models:

- **(TCII–S1)** No Arc Damage Scenario in the TS.
- **(TCII–S2)** One-Arc Damage Scenario in the TS.
- **(TCII–S3)** Two-Arc Damage Scenario in the TS.

3. **Test Case III (TCIII)**, presented in section 4.2.3, investigates the performance of the models **MSO-MRT** and **MSO-MPL** under different repair time scenarios to mend a damaged branch. We aim to demonstrate and analyze how a workforce shortage (e.g., due to health emergencies caused by a pandemic crisis) or hardship in the repair process (e.g., due to adverse weather conditions or limited accessibility to the damaged area) affects the performance of the proposed models in effectively restoring service in the face of an HILP event. This is captured through different realizations of the repair time for damaged branches in the DS. The proposed models still coordinate the use of MPS technologies with RC dispatch over the entire restoration horizon, taking into account the constraints in the TS. To highlight the role of the repair time in DS restoration and resilience, we limit the analysis in **TCIII** to a one-branch damage scenario in the DS (similar to **TCI-S1**), but under different arc damage scenarios in the TS and repair times for the damaged branches. The time needed for RCs to repair a damaged branch in the DS is considered variable ranging from 6 time periods (30 minutes) to 24 time periods (2 hours), while the damaged arcs in the TS are considered unavailable during the entire restoration process. The following four scenarios (S) are investigated in **TCIII** for both **MSO-MRT** and **MSO-MPL** models:
   - **(TCIII–S1)** Six-period Repair Time Scenario for Damaged Branches in the DS.
   - **(TCIII–S2)** Twelve-period Repair Time Scenario for Damaged Branches in the DS.
   - **(TCIII–S3)** Eighteen-period Repair Time Scenario for Damaged Branches in the DS.
   - **(TCIII–S4)** Twenty-Four-period Repair Time Scenario for Damaged Branches in the DS.
4. **Test Case IV (TCIV)**, presented in section 4.2.4, investigates the choice of the DS restoration approaches and compares the performance of the models **MSO-MRT** and **MSO-MPL** with several existing technologies and conventional practices for DS restoration. In particular, we aim to demonstrate and highlight the value of *resource mobility* and also joint network and resource coordination in the DS restoration process against the stationary and singular focuses on the existing restoration practices. To investigate and highlight the choice of the restoration approach, we apply all conventional and proposed restoration approaches to a given HILP realization (the same as that in **TCI-S3**) under the following assumptions: (i) three-branch damage scenario in the DS, (ii) no disruption in the TS, (iii) eight-period repair time for damaged branches in the DS. The following five scenarios (S) are investigated in **TCIV** for both **MSO-MRT** and **MSO-MPL** models:
   - **(TCIV–S1)** Conventional DS Restoration via RCs Only.
   - **(TCIV–S2)** Conventional DS Restoration via RCs and SEGs.
   - **(TCIV–S3)** Proposed DS Restoration via RCs and MEGs.
   - **(TCIV–S4)** Proposed DS Restoration via RCs and MESSs.
   - **(TCIV–S5)** Proposed DS Restoration via RCs, MEGs, and MESSs
5. **Test Case V (TCV)**, presented in section 4.2.5, investigates the performance of the proposed **MSO-MRT** and **MSO-MPL** models when the number of MPS resources are doubled and tripled. We aim to demonstrate and analyze how an increase in the number of the available MPSs affects the performance of the proposed models in effective service restoration in the face of an HILP incident. To highlight the role the varying availability of MPS units plays on DS restoration and resilience, we limit the analysis in **TCV** to a given HILP realization (the same as that in **TCI-S3**) under the following assumptions: (i) three-branch damage scenario in the DS, (ii) no disruption in the TS, (iii) eight-period repair time for damaged branches in the DS. The following two scenarios (S) are hence investigated in **TCV** for both **MSO-MRT** and **MSO-MPL** models:
   - **(TCV–S1)** Double the number of available MPSs — 6 MPSs (4 MEGs & 2 MESSs).
   - **(TCV–S2)** Triple the number of available MPSs — 9 MPSs (6 MEGs & 3 MESSs).

6. **Test Case VI (TCVI)**, presented in section 4.2.6, investigates the performance of the models **MSO-MRT** and **MSO-MPL** when an HILP event causes more severe damages. In order to highlight the impact of more serve damages in both DS and TS for DS restoration and resilience, our analysis in **TCVI** is based on a four-branch damage scenario in the DS, but under different routing availability assumptions in the TS. The time needed for the RCs to mend any damaged branches in the DS is eight periods of five minutes, while the damaged arcs in the TS are unavailable during the entire restoration process. The number of available MPSs is three — two MEGs and one MESS. The two scenarios (S) below are investigated in **TCVI** for both **MSO-MRT** and **MSO-MPL** models:
   - **(TCVI–S1)** One-Arc Damage Scenario in the TS.
   - **(TCVI–S2)** Two-Arc Damage Scenario in the TS.

In the next sections, we numerically investigate the above-introduced test cases and scenarios using the proposed **MSO-MRT** and **MSO-MPL** models and, accordingly, provide the insights gained.

4.2.1. TCI: Impact Analysis of Different DS Branch Damage Scenarios. The objective is here to demonstrate and analyze how the proposed models coordinate the use of MPS technologies with RC dispatch over the entire restoration time horizon so as to optimally achieve the expected objectives of resilience in the DS. We have created four-branch damage scenarios in the DS. We recall that the TS network is here assumed fully available. The DS restoration is pursued in joint coordination of the DS and TS networks. The available resources to achieve this goal are one RC and three MPSs (two MEGs and one MESS). The repair time for each damaged branch is assumed to be eight periods (40 minutes). The studied scenarios in **TCI** are listed in Table 2.

Table 2 Studied DS Branch Damage Scenarios in TCI

Scenarios	Damaged branches
TCI–S1	$L1(n1-n2)$
TCI–S2	$L1(n1-n2)\&L25(n6-n26)$
TCI–S3	$L1(n1-n2)\&L8(n8-n9)\&L25(n6-n26)$
TCI–S4	$L1(n1-n2)\&L8(n8-n9)\&L22(n3-n23)\&L25(n6-n26)$

The optimal schedules of MPSs/RC during the restoration process are shown in Figures 8 and 9, respectively, for the models **MSO-MRT** and **MSO-MPL**. For the sake of further clarity, we here discuss details of **TCI–S3** (Figure 8) where model **MSO-MRT** is used. In this scenario, three DS branches (i.e., L1, L8, and L25) are damaged and offline due to an HILP incident, resulting in the outage of the entire set of DS nodes. At the beginning of the restoration process, the available resources (1 RC and 3 MPSs) are prepositioned at the emergency center (EC) at TS node 1 (see Figure 7). At $t = 1$, MEG1 and MESS1 start traveling and reach their destination (DS node 3) at $t = 5$ while RC leaves at $t = 1$ to reach its destination (damaged line L1) at $t = 5$. All resources remain in service for eight periods until $t = 12$ when line L1 is repaired. Starting from $t = 13$, (i) MEG1 travels for ten periods across the TS to reach and deliver power to the DS node 9 at $t = 23$, (ii) MESS1 travels for 14 periods to reach and deliver power to DS node 9 at $t = 27$, and RC travels for five periods and mend branch L25 at $t = 18$. In the meantime, MEG2 is called at $t = 21$, travels for four periods, and starts delivering power to node 12 at $t = 25$. With the help of all 3 MPS technologies, the second damaged branch L25 is fixed at $t = 25$ and the DS is fully restored at $t = 26$ (indicated in blue), while the third damaged branch L8 is yet to be fixed. This highlights the role of MPS technologies in aiding a faster DS restoration compared to the traditional RC-only strategies and avoids the significant economic losses and societal discomfort that could arise from a prolonged electricity outage. While the DS is fully restored at $t = 26$, (i) MEG1 stays connected delivering power to DS node 9 for 10 additional periods until $t = 35$, (ii) MEG2 stays connected to DS node 12 for ten additional periods until $t = 35$, (iii) MESS1 remains connected to the DS node 9 at $t = 27$, and delivers power for nine periods until $t = 35$, and (iv) RC travels for two periods, repair the third damaged branch L8 starting from $t = 28$ for eight periods until $t = 35$. At $t = 35$, all three damaged branches are fixed, the entire DS returns to its normal operating condition, and the MPS/RC services are no longer needed.

Figure 8 shows that the DS full restoration is achieved at $t = 13$ in **TCI–S1** and at $t = 26$ in **TCI–S2**, in both cases when all damaged branches are fixed by RCs. That is, the MPSs utilized in these two scenarios could only help the service restoration at some individual nodes, while the full DS restoration is credited to the RCs that repaired all the damaged branches in the DS. On the other hand, the DS full restoration is achieved at $t = 26$ in **TCI–S3** and at $t = 34$ in **TCI–S4**, while several damaged branches are yet to be fixed. This highlights the critical role of MPS technologies in DS restoration when the number of damaged branches increases and outage scenarios are more severe. In particular, one expects to realize a longer DS restoration time when the number of damaged branches increases. However, comparing the results in **TCI–S2** with two damaged branches and **TCI–S3** with three, one can see that the same restoration time ($t = 26$) is achieved

Figure 8 Optimal MPSs/RCs Schedules During the Restoration Process: MSO-MRT [Color figure can be viewed at wileyonlinelibrary.com]

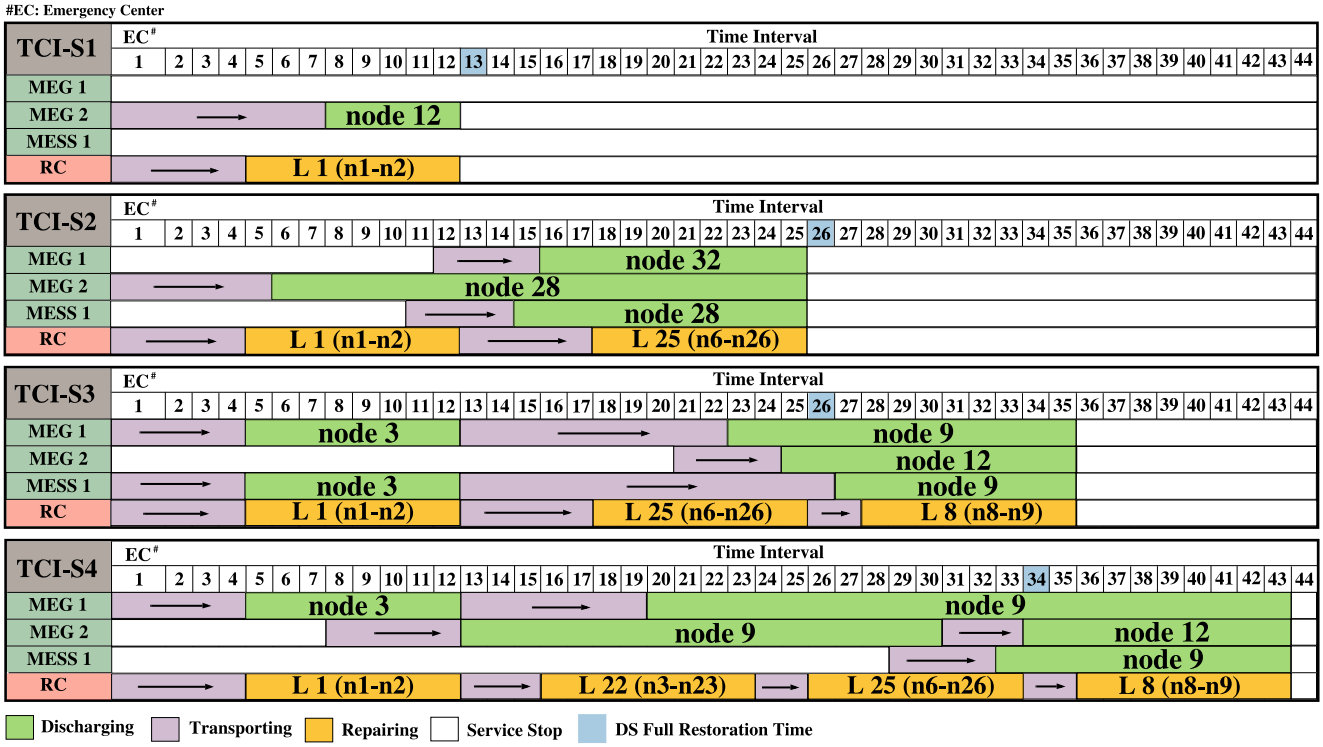

Figure 9 Optimal MPSs/RCs Schedules During the Restoration Process: MSO-MPL [Color figure can be viewed at wileyonlinelibrary.com]

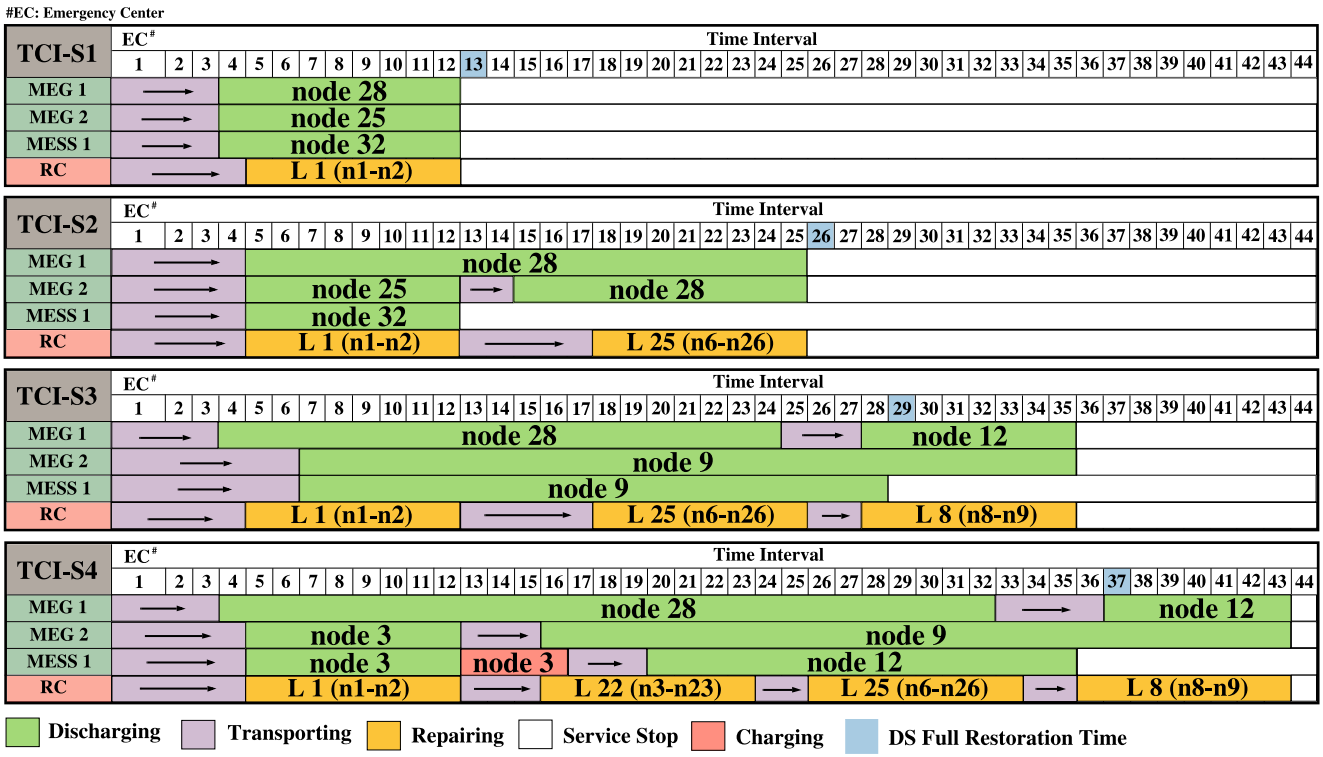

primarily thanks to the effective utilization of MPS technologies in the latter. Furthermore, Figure 8 conveys that, common to all studied scenarios in **TCI**, the MESS utilization during the DS restoration process is more limited than that of MEGs. The reason lies in the objective function in model **MSO-MRT** which

minimizes the DS restoration time. Accordingly, and different from MEGs with no charging capabilities, MESS is less utilized due to possible needs to travel to charging stations and its charging requirements which may further delay the restoration process.

Figure 9 presents the RC and MPS routing and scheduling with model **MSO-MPL**. As in Figure 8, DS restoration is achieved by reparation of the damaged branches in the first two scenarios (**TCI–S1** and **TCI–S2** with one and two damaged branches, respectively), while MPSs contribute to a faster DS restoration in the last two scenarios (**TCI–S3** and **TCI–S4** with three and four damaged branches, respectively). That is, effective utilization of MPSs leads to a much earlier full DS restoration than when all the damaged branches are mended. Model **MSO-MPL** uses MESSs more intensively in the restoration process.

The results on **TCI–S4** (Figure 9) illustrate that the MESS has requested a charging service for four periods at the same node (i.e., node 3) it was earlier providing power to, allowing for the service of another outage node (i.e., node 12) in the next periods. Note that MESS charging at DS node 3 takes place at $t = 13$ when branch L1 is mended and node 3 is hence fully recovered.

Observation 1. *The above results demonstrate the effectiveness of the MPS technologies in achieving a faster full DS restoration compared to the traditional RC-only practices even while one or several damaged branches are yet to be fixed. This observation holds, irrespective of the considered model (**MSO-MRT** or **MSO-MPL**) and the number of damaged branches in the DS, due to the ability of the MPSs to provide enough power while the RC is fixing the damaged branches. This observation is particularly highlighted in scenarios involving multiple damaged branches in the DS, common to the majority of the HILP incidents.*

Observation 2. *The choice of the objective function greatly impacts MPS/RC routing and scheduling decisions and the frequency and extent of their involvement in the DS restoration process. The proposed model **MSO-MPL** utilizes MPSs more frequently and intensely than model **MSO-MRT** during the restoration process. The nature of the **MSO-MPL** model that minimizes the lost power incentivizes the accrued use of MESS. This is in contrast with the **MSO-MRT** model, where the charging duration and requirements of MESS may not allow to effectively achieve the model's objective, that is, minimal DS restoration time.*

Observation 3. *The choice of objective function greatly impacts the restoration duration and process. The **MSO-MRT** model achieves a faster full service restoration across the entire DS. However, the **MSO-MPL** model effectively allows for partial recovery of the system and the faster recovery of particular outage nodes, if needed. This is of general interest as there commonly exist critical nodes in the DS (e.g., hospitals, military bases, fire stations) whose quick restoration is fundamental.*

4.2.2. TCII: Impact Analysis of Different TS Arc Disruption Scenarios. We aim to demonstrate and analyze how the proposed models coordinate the use of MPS technologies with RC dispatch and take into account the constraints in the TS, that is, potential unavailability of TS arcs due to an HILP event. This is a critical aspect of this study as our goal is to harness the mobility of MPS technologies for DS restoration, in which the TS plays a critical and interdependent role. The available resources to achieve this goal are one RC and three MPSs (two MEGs and one MESS) technologies. We focus on a base condition where an HILP event has caused a three-branch damage scenario in the DS, that is, the simultaneous failure of L1, L8, and L25. The repair time for each damaged branch is assumed to be eight periods (40 minutes). We have created three scenarios to study the effects of TS arcs damage and/or unavailability in the DS restoration process, the detailed information on which is provided in Table 3.

Under the above assumptions, the impact of TS arc disruptions on the DS restoration performance can be visualized in Figure 10. According to Figure 10, TS disruptions generally result in an increase in the time needed to achieve a full DS restoration. Additionally, comparing the results of both models clearly demonstrates that in all scenarios in general and for **TCII–S3** in particular, the **MSO-MPL** model provides a smoother restoration process than the **MSO-MRT** model. We here highlight the role of TS constraints in the DS restoration process. With model **MSO-MRT**, a sudden change in service restoration can be observed in **TCII–S3** at $t = 26$. Considering the unavailability of two TS arcs in this scenario and, accordingly, the potentially higher travel time for the MPS to reach the desired node—since the shortest path in the TS might not be available—model **MSO-MRT** does not utilize MPS technologies until later during the restoration horizon at $t = 20$. This is in line with the objective of the **MSO-MRT** model to minimize the time it takes to full DS restoration. The sudden change in the service restoration performance at $t = 25$ is explained by the arrival of several MPSs to contribute to the response and recovery process. This is, however, not the case for **TCII–S1** and **TCII–S2** where MPSs are assigned to contribute to the restoration process by traveling to the adjacent TS nodes with minimal travel time.

Table 3 Details of Scenarios Studied in TCII

DS damaged branch	Scenarios	Transportation arc failure
L1(n1-n2) & L8(n8-n9) & L25(n6-n26)	TCII–S1	—
	TCII–S2	A1(1-2)
	TCII–S3	A1(1-2) & A2(3-12)

OBSERVATION 4. *The service restoration curve in Figure 10 demonstrates that the TS constraints and potential disruptions during HILP events significantly affect the MPSs' and RC travel time, their assignments, dispatch, and contribution in the DS restoration process. Depending on the model selected and the objective to optimize, one may achieve a smoother restoration performance across the DS with more involvement of MPS early on during the restoration process (in case of* ***MSO-MPL****), or radical improvements in the DS service restoration at the later times during the restoration process and by less involvement of MPS in general (in case of* ***MSO-MRT****).*

Figure 10 Impact of TS Disruptions on DS Service Restoration—3-Branch Damage Scenario in the DS [Color figure can be viewed at wileyonlinelibrary.com]

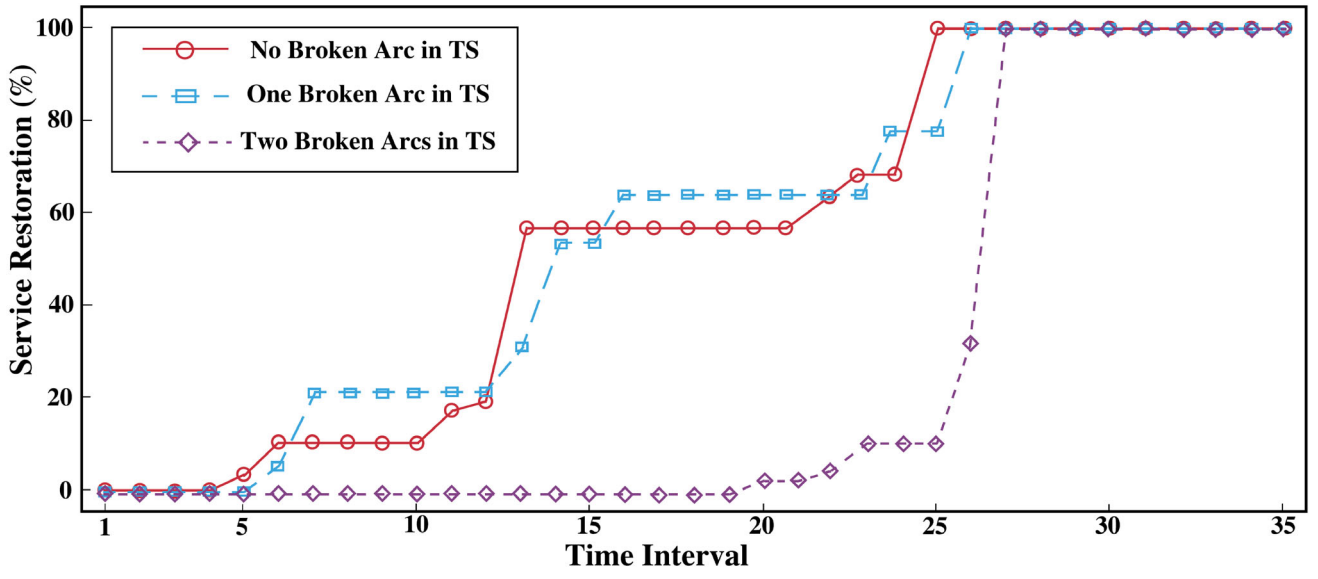

(a) MSO-MRT

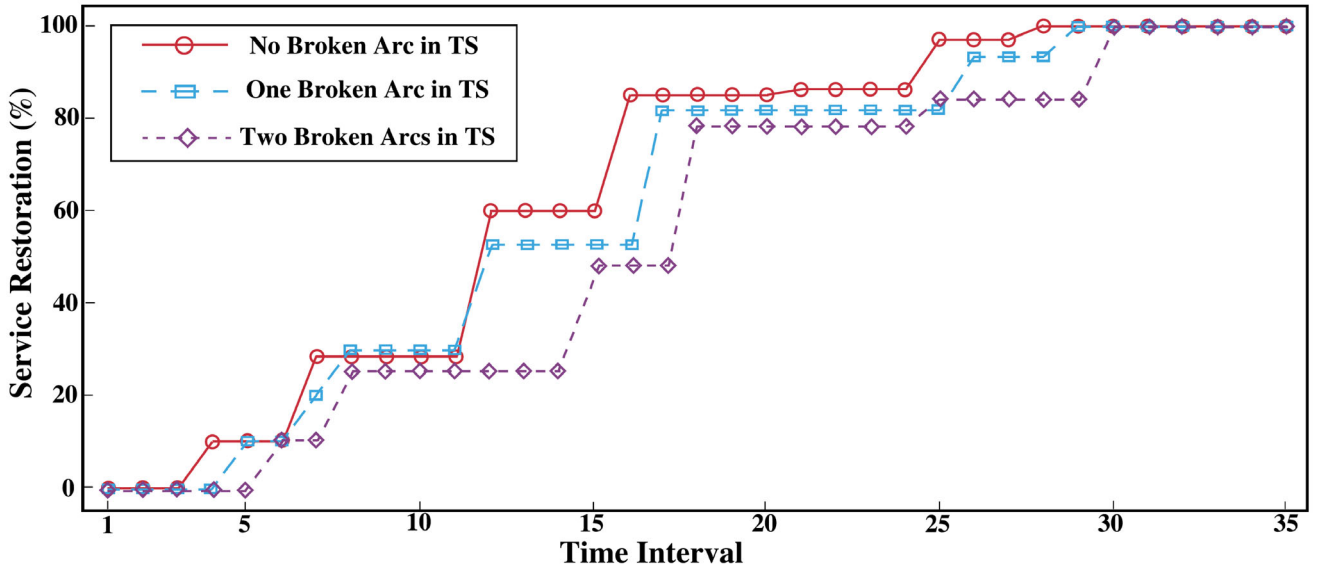

(b) MSO-MPL

4.2.3. TCIII: Impact Analysis of Different Repair Time Scenarios. The change in the repair time can be due in practice to a staffing shortage (e.g., personnel health emergencies, pandemic crisis) or the hardship of the repair process (e.g., adverse weather conditions or limited accessibility to the damaged area). We evaluate here the effectiveness of the **MSO-MRT** and **MSO-MPL** models as a function of the time needed to mend a DS damaged branch. In so doing, we focus on a single-branch damage scenario in the DS (i.e., the failure of L1 connecting DS node 1 to DS node 2) and analyze the four TS disruption scenarios listed in Table 4. Note that the studied DS failure is a non-trivial, most-critical system failure resulting in outages spanning the entire DS. The available resources to achieve the DS restoration goal are one RC and three MPSs (two MEGs and one MESS).

The minimal DS restoration time in different scenarios, obtained from the proposed **MSO-MRT** and **MSO-MPL** models, is displayed in Figure 11. As one can see, the DS restoration time for L1 failure in the DS remains the same in all studied scenarios when using **MSO-MRT** and **MSO-MPL** models. This is because the reparation of the damaged branch L1 results in a full restoration of the DS and that the total MPS capacity is not sufficient to account for the entire DS restoration before the damaged branch L1 is mended. The DS restoration time increases as the repair time of the damaged branches increases. Additionally, one can observe that the DS restoration time increases up to 20% (**TCIII-S1**) when taking into account the transportation arc failures. In particular, every additional arc failure in the TS leads to a one-period increment for restoring the DS. The longest DS restoration time is achieved in **TCIII-S4** when considering the longest repair time for a damaged branch in the DS (120 minutes) in the presence of two broken arcs in the TS. In all studied scenarios in **TCIII**, the coordination between the TS and DS and the joint utilization of mobile resources have resulted in full restoration of the DS within the desired 4-hour restoration time horizon. Note that while the goal was the entire DS restoration, individual nodes may have been restored earlier with the MPSs being dispatched across the DS.

Table 4 Details of Scenarios Studied in TCIII

DS Damaged Branch	Scenarios	Repair time (min)	Transportation arc failure
L1 (n1-n2)	**TCIII–S1**	30	—
			A1(1-2)
			A1(1-2) & A2(3-12)
	TCIII–S2	60	—
			A1(1-2)
			A1(1-2) & A2(3-12)
	TCIII–S3	90	—
			A1(1-2)
			A1(1-2) & A2(3-12)
	TCIII–S4	120	—
			A1(1-2)
			A1(1-2) & A2(3-12)

Figure 11 Minimum Time for DS Restoration under Different Repair Time Scenarios for DS Damaged Branch L1: Results with MSO-MRT and MSO-MPL [Color figure can be viewed at wileyonlinelibrary.com]

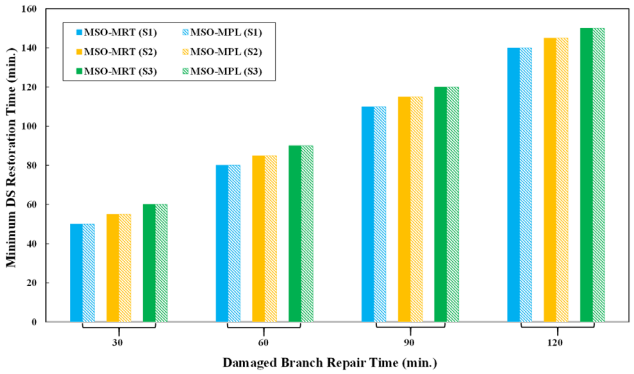

Figure 12 provides the same analysis when applied to a double-order contingency event in the DS: the simultaneous failure of DS branches L8 and L25. Similar observations to those found in Figure 11 prevail, except that in this case, the minimum DS restoration time achieved using the **MSO-MRT** and **MSO-MPL** models differ in every studied instance. As expected, a faster DS restoration is commonly achieved when the **MSO-MRT** model is used. With the restoration planning horizon set to 48 periods (four hours), the full DS restoration cannot be achieved when the repair time for damaged branches increases to two hours; this is primarily due to the necessary travels that RCs and MPSs should make to reach the desired area (arc and node), which does not leave sufficient time required for a full restoration neither through MPS contributions nor reparation of the damaged branches.

OBSERVATION 5. *The minimum DS restoration time is in a direct and linear relationship with the repair time of the damaged branches in the DS, irrespective of the model (**MSO-MRT** or **MSO-MPL**) used. However, the minimum DS restoration time in particular cases (e.g., failure in the most critical branch in the DS—the root branch L1) may remain the same for both **MSO-MRT** and **MSO-MPL** models under all studied scenarios, while it may be model-dependent in some other instances. If the repair time for damaged branches in the DS exceeds a threshold, the results demonstrated that a full DS restoration may not be achieved. This highlights the necessary adjustments and reinforcements needed to strengthen the*

Figure 12 **Minimum Time for DS Restoration under Different Repair Time Scenarios for DS Damaged Branches L8-L25 : Results with MSO-MRT and MSO-MPL [Color figure can be viewed at wileyonlinelibrary.com]**

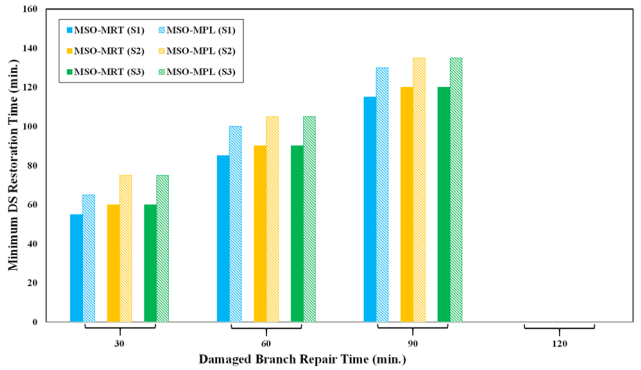

response and recovery process when the repair time is uncertain or estimated to be longer than expected (e.g., unavailability or inaccessibility of damaged equipment, shortage in RC workforce).

4.2.4. TCIV: Impact Analysis of Different Restoration Strategies. We have created five scenarios and have used models **MSO-MRT** and **MSO-MPL** to study the effectiveness of the different restoration approaches. We are especially interested in comparing the proposed mobility-as-a-service ideology with the current business-as-usual practice and existing technologies. The existing DS restoration technologies are taken as RC-Only practices and the use of SEG. We assume here that the TS is fully operational and not affected by HILP incidents. We focus on DS restoration in response to extensive outages in the DS caused by the failure of three branches: L1 connecting DS nodes 1 to 2, L8 connecting DS nodes 8 to 9, and L25 connecting DS nodes 6 to 26. The repair time for each damaged branch is assumed to take 40 minutes. Detailed information on the studied scenarios in **TCIV** is provided in Table 5.

Figures 13a–c illustrate the results obtained with the proposed models **MSO-MRT** and **MSO-MPL**. They display the time taken to restore power in the entire DS with various restoration approaches and under different assumptions of power capacity for the energy resources (i.e., lower to higher power capacity in (a)–(c)). The restoration approaches include two of the existing practices and three transportable sources —**TCIV-S3**: MEG, **TCIV-S4**: MESS, and **TCIV-S5**: MPS (i.e., MEG + MESS). In every studied scenario, the RC schedules are coordinated with the respective technology, thereby creating a joint contribution to DS service restoration. Figure 13a demonstrates that the conventional RC-Only (**TCIV–S1**) and RC-SEG (**TCIV–S2**) practices result in the longest DS restoration time compared to the proposed RC-MEG (**TCIV–S3**) and RC-MPS (**TCIV–S5**) strategies. Irrespective of the selected model **MSO-MRT** or **MSO-MPL**, this observation remains valid as the capacity of the power sources increase in 13 (b)-(c). Moreover, as the power capacity of the MPS sources increase, the contribution of MPS to restore power is further highlighted compared to the traditional practices.

Table 5 **Details of the Studied Scenarios in TCIV**

Scenarios	Restoration technology	Specification
TCIV–S1	**RC-Only**	–
		–
		–
TCIV–S2	**RC + SEG**	400 kW/300 kVar (*n*6 & *n*28)
		500 kW/500 kVar (*n*6 & *n*28)
		800 kW/600 kVar (*n*6 & *n*28)
TCIV–S3	**RC + MEG**	400 kW/300 kWh
		500 kW/500 kVar
		800 kW/600 kVar
TCIV–S4	**RC + MESS**	300 kW/500 kWh
		500 kW/776 kWh
		600 kW/1000 kWh
TCIV–S5	**RC + MPS**	400 kW/300 kVar + 300 kW/500 kWh
		500 kW/600 kVar + 500 kW/776 kWh
		800 kW/600 kVar + 600 kW/1000 kWh

OBSERVATION 6. *The results presented in Figure 13a–c showcase the advantage of the proposed MPS technologies compared to the existing practice. MPS technologies, particularly when their size and capacity increase, are able to play a critical role in picking up the load in DS restoration. Additionally, the results confirmed our previous observation that when the DS system-wide (and not at particular nodes) restoration time is of interest, model* ***MSO-MRT*** *outperforms model* ***MSO-MPL****.*

We focus now on model **MSO-MPL** to investigate the role of different strategies in service restoration at particular nodes in the DS. Figure 14 shows that the MPS technologies consistently allow for a faster restoration of the DS nodes of interest compared to the traditional practices. One can see that the fastest recovery of the DS node 28 is achieved with an SEG because it is connected locally to node 28.

OBSERVATION 7. *The results presented in Figure 14 demonstrate the significant advantages of MPS technologies in the restoration of individual DS nodes over the traditional RC-only and SEG practices. When restoration of particular (critical) nodes—and not the entire DS—is of interest, model* ***MSO-MPL*** *best harnesses the MPS potential in the restoration of critical nodes and mission-critical systems.*

Figure 13 DS Restoration Time vs. Restoration Strategy: Results with MSO-MRT and MSO-MPL [Color figure can be viewed at wileyonlinelibrary.com]

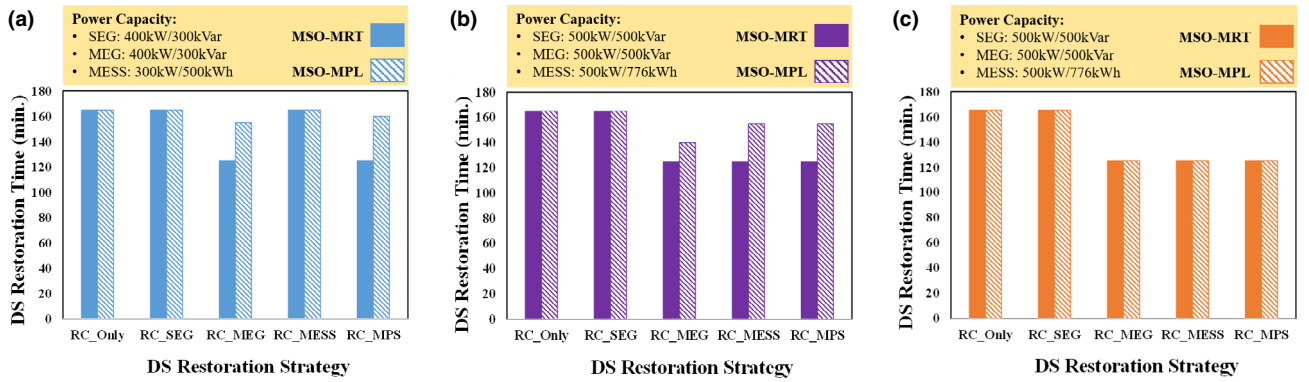

Figure 14 Nodal Restoration Time under Different Strategies [Color figure can be viewed at wileyonlinelibrary.com]

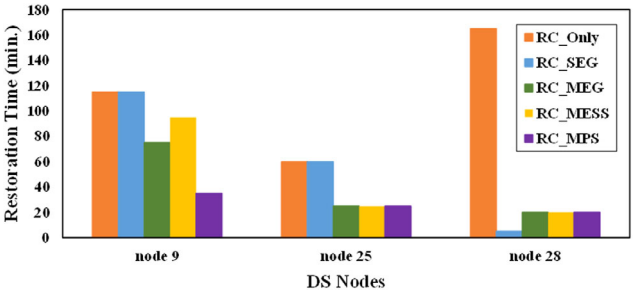

4.2.5. TCV: Impact Analysis of Variable Availability of MPS Units. We have generated two scenarios and have used models **MSO-MRT** and **MSO-MPL** to evaluate the effect of varying numbers of available MPSs for DS restoration. We assume here that the TS is fully operational and not affected by the HILP incident. We concentrate on DS restoration in response to extensive outages in the DS caused by the failure of three branches: L1 connecting DS nodes 1 to 2, L8 connecting DS nodes 8 to 9, and L25 connecting DS nodes 6 to 26. The repair time for each damaged branch is assumed to take 40 minutes. The number of MPSs is six (i.e., four MEGs and two MESSs) in **TCV-S1**, while it is nine (i.e., six MEGs and three MESSs) in **TCV-S2**. Table 6 presents the results obtained with the models **MSO-MRT** and **MOS-MPL**. The results displayed in Table 6 indicate that:

- The utilization of MPSs leads to a much faster full DS restoration (130 minutes) than when all the damaged branches in the DS are mended (175 minutes); that is an improvement of 34.6% in achieving a full system restoration when MPS technologies are applied.
- The minimal times for full DS restoration are the same in both models **MSO-MRT** and **MSO-MRL** with a sufficient number of MPSs. One can see that the full restoration times are the same when the number of MPS resources are doubled and tripled. Moreover, increasing the number of MPS resources comes at a significant price, thereby calling for an effective trade-off between the investment/operational costs and the DS restoration agility.

These results confirm the effectiveness of the MPS technologies to achieve a faster full DS restoration compared to the conventional practices, which corroborates **Observation 1**.

4.2.6. TCVI: Impact Analysis of More Severe Damages in DS and TS. We aim to demonstrate and analyze the performance of the proposed models **MSO-MRT** and **MSO-MPL** under (more) severe damages in the DS and TS caused by an HILP event. The available resources to achieve this goal are one RC and three MPSs (i.e., two MEGs and one MESS) technologies. The repair time for each damaged branch is assumed to be eight time periods (40 minutes). We focus on a severe condition where an HILP event has caused a four-branch damage scenario in DS: L1 connecting DS nodes 1 to 2, L8 connecting DS nodes 8 to 9, L22 connecting DS nodes 3 to 26, and L25 connecting DS nodes 6 to 26. We have created two scenarios under one-arc damage in the TS (**TCVI-S1**) and two-arc damage in the TS (**TCVI-S2**). Table 7 presents the results obtained with the proposed models **MSO-MRT** and **MOS-MPL**. It illustrates that:

- The utilization of MPSs results in a much earlier full DS restoration than when all the damaged branches are eventually fixed.

Table 6 Time for Restoration under Different Numbers of MPSs in TCV

		Time for full electrical restoration	Time for full structural restoration (all damaged branches fixed)
TCV–S1	**MSO-MRT**	26-period (130 min)	35-period (175 min)
	MSO-MPL	26-period (130 min)	35-period (175 min)
TCV–S2	**MSO-MRT**	26-period (130 min)	35-period (175 min)
	MSO-MPL	26-period (130 min)	35-period (175 min)

Table 7 Time for Restoration under More Severe Damage in DS and TS in TCVI

		Time for full electrical restoration	Time for full structural restoration (all damaged branches fixed)
TCVI–S1	**MSO-MRT**	34-period (170 min)	44-period (220 min)
	MSO-MPL	37-period (185 min)	44-period (220 min)
TCV–S2	**MSO-MRT**	36-period (180 min)	47-period (235 min)
	MSO-MPL	39-period (195 min)	47-period (235 min)

- **MSO-MRT** model achieves a faster full restoration across the entire DS than **MSO-MPL** model.
- The time for full DS restoration increases when the HILP event results in a more severe damage in the DS and TS.

Again, these results are consistent with **Observation 1**, **Observation 3**, and **Observation 4** reported earlier for **TCI** and **TCII**.

4.3. Test System Description: Test System 2

In order to verify the versatility and applicability of the proposed models in systems with larger geographical coverage, we introduce a new benchmark test system as in Xu et al. (2019). The configuration of the new test systems is illustrated in Figure 15, where the DS and TS networks are integrated through several coupling nodes defined in Table 8. The DS network is the IEEE 33-node test system which includes 1 substation, 32 branches, and 33 nodes serving a total electricity demand of 3,715 kW. The detailed information on each node and branch in the system is provided by Baran and Wu (1989). The TS network is called the Simplified Electrified TS network and consists of 12 nodes and 20 arcs, in which a total of six candidate nodes and four coupling nodes mapped to four DS repair zones around specific branches exist. For more detailed information about the network, we refer the reader to Xu et al. (2019).

Due to the increased distance between nodes in the Simplified Electrified TS Network, we explore a 50%-longer planning horizon for service restoration in this test system. The entire restoration time horizon in all the conducted tests on this test system is assumed to be 72 periods of five minutes (6 hours) compared to 48 periods in the first test system. We aim to test and investigate the performance of the proposed **MSO-MRT** and **MSO-MPL** models in all test cases on this system configuration (96 test instances in total).

4.4. Numerical Results and Insights: Test System 2

This section summaries the findings and contributions made for Test System 2. We verify the effectiveness of the presented schemes for DS restoration applying the same six test cases presented in section 4.2. The test cases and the detailed numerical results are provided in Appendix C. The analysis of the proposed models applied to Test System 2 leads to the following conclusions:

- The results show the effectiveness of the MPS technologies in achieving a faster full DS restoration compared to the traditional RC-only practices even while one or several damaged branches are yet to be fixed. This observation holds irrespective of the considered model (**MSO-MRT** or **MSO-MPL**) and the number of damaged branches due to the ability of the MPSs to provide enough power while the RC is fixing the damaged branches. This observation is especially visible in scenarios involving multiple damaged branches in the DS, a feature common to most HILP incidents.
- The choice of objective function greatly impacts the restoration duration and process. In scenarios with multiple damaged branches in the DS, the **MSO-MRT** model achieves a full-service restoration around 5 to 30 minutes earlier across the entire DS due to the nature of the objective function, which aims to achieve minimal DS restoration time. When the number of MPS resources are sufficient (i.e., more than six), the minimal times for full DS restoration are the same in both **MSO-MRT** and **MSO-MRL** models.
- The TS constraints and disruptions during HILP events significantly affect the MPSs' and RCs' travel time, their assignments, dispatch schedules, and contribution to the DS restoration process. The more severe a disruption in the TS, the more time needed to achieve a full restoration.
- The minimum DS restoration time is in a direct and linear relationship with the repair time of the damaged branches in the DS, irrespective of the model (**MSO-MRT** or **MSO-MPL**) used.
- MPS technologies, particularly when their size and capacity increase, are able to play a critical role in picking up the load for DS restoration. This highlights the advantage of the proposed

Figure 15 Configuration of the Integrated TS and DS Networks in Test System 2 [Color figure can be viewed at wileyonlinelibrary.com]

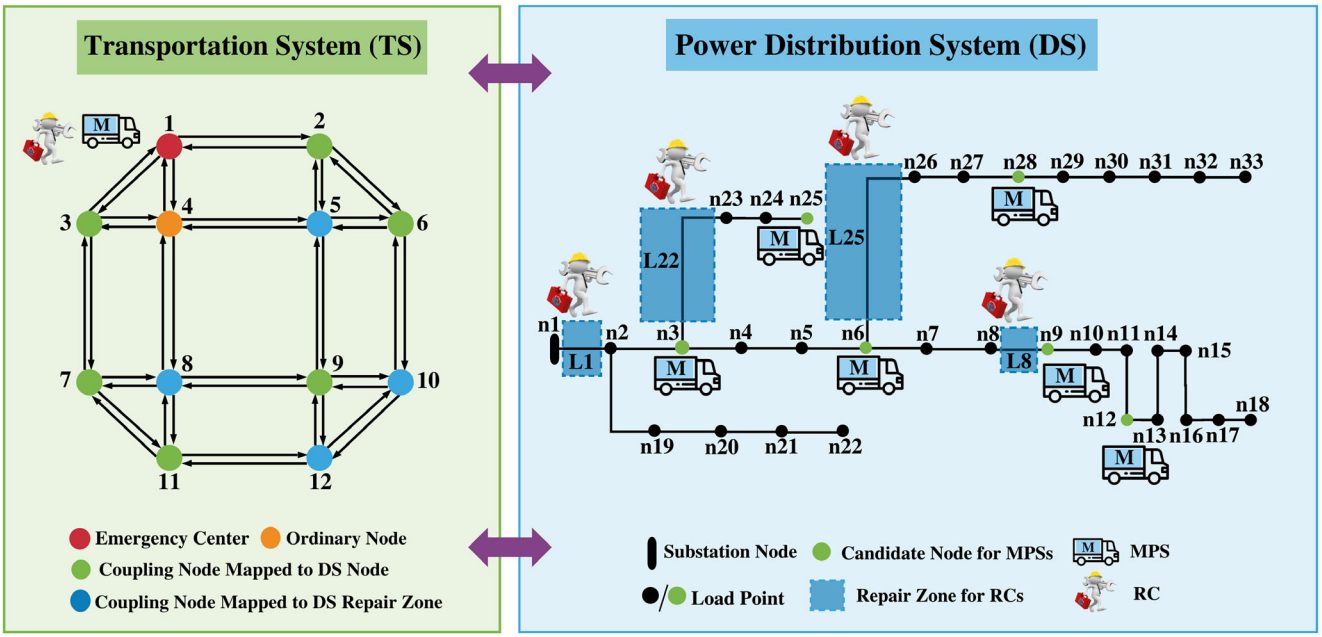

Table 8 Coupling Points in the Integrated TS and DS Networks in Test System 2

TS nodes	DS candidate nodes	TS nodes	DS repair zones
2	*n*3	5	*L*1(*n*1–*n*2)
3	*n*6	8	*L*22(*n*3–*n*23)
6	*n*28	10	*L*8(*n*8–*n*9)
7	*n*25	12	*L*25(*n*6–*n*26)
9	*n*9		
11	*n*12		

MPS technologies compared to the traditional restoration practices.

The presented findings endorse the results obtained in section 4.2 and confirm the effectiveness of the MPS technologies in achieving a faster full restoration and enhanced DS resilience to HILP incidents.

5. Discussions and Conclusion

Power interruptions following an extreme HILP event in the DS must be restored quickly to minimize the disastrous consequences of prolonged outages to the society and provide stable operations to emergency centers, hospitals, military bases, fire stations, etc. Decision-making for DS service restoration has long been a challenge for the electric industry. Service restoration decisions for the DS are commonly approached through maintenance and repair activities of the damaged infrastructure by using RCs or by deploying SEGs. In the former case, the restoration process may take days and significantly harm people and every aspect of our electrified economy. In the latter case, SEGs can best help restore a single facility for a limited period of time. Different from the state-of-the-art practices, this study introduces mobility-as-a-service for resilience delivery and proposes the effective deployment of MPS as the restoration technology of the future. The transportability of MPSs can be harnessed for spatiotemporal flexibility exchange and effective response and recovery during disasters. MPSs not only facilitate a faster DS restoration compared to the aforementioned traditional practices, but also may support the energy-intensive facilities and electricity delivery to mission-critical systems and emergency services locally until the system is returned back to its normal operating condition.

While MPSs can accelerate the response and recovery of the DS in the face of HILP events, their potential for delivering resilience services has remained largely untapped and they are currently not well utilized in practice. Their operation should be coordinated in space and time as well as with other available resources. To fill in this gap in the literature, we propose two optimization models that integrate both DS and TS constraints into a unified framework and provide informative decisions on the coordinated operation of MPS and RC resources for DS restoration. With a view toward Industry 4.0 and 5.0 technological advancements, opportunities will evolve for automation of MPSs priority services with the goal to strike a balance between machines and humans working hand-by-hand during the service restoration process when an HILP event adversely affects the society and its critical infrastructure.

5.1. Managerial Insights Summary

Through six test cases, we have extensively analyzed the MPS technologies under the lens of the proposed optimization models **MSO-MRT** and **MSO-MPL** in two different test systems. With the designed test cases, each with a multitude of scenarios, we evaluated (i) the performance of the models in multi-branch damage scenarios in the DS, (ii) the impact of TS arc disruptions on the DS restoration performance, (iii) the impact of variable repair time scenarios on the DS restoration, (iv) the choice of restoration strategy and a comparison with the traditional approaches and the existing practices, (v) the variable availability of MPS resources, and (vi) more severe disruptions in both DS and TS. We consistently observed the value of MPS technologies in general and their mobility in particular for spatiotemporal resilience delivery across the DS. We found that MPS technologies almost always outperform the conventional settings when the focus is to minimize the time it takes to achieve a full DS restoration. Among our findings are the following insights:

- Different from the traditional RC-only practices, MPSs facilitate the full DS restoration even while one or several damaged branches are yet to be fixed. This is especially valuable in scenarios involving multiple damaged branches in the DS, common to the majority of HILP incidents.
- The choice of the objective function greatly impacts the MPS/RC routing and scheduling decisions: how frequently they are utilized and how involved their utilization is during the DS restoration process. The **MSO-MRT** model achieves a *faster* service restoration across the entire DS. However, the **MSO-MPL** model effectively allows for partial recovery of the system and the faster recovery of particular outage nodes, if needed. This is particularly valuable as it offers opportunities to swiftly restore the critical loads such as hospitals, military bases, fire stations.
- The TS route disruptions and unavailability due to HILP events greatly affect the MPSs' and RC travel time, their assignment, dispatch, and contribution in the DS restoration process. With disruptions in TS, MPSs/RCs may get dispatched through alternative (and not necessarily the shortest) routes. Our analysis highlighted the need for integration of TS and DS constraints into a unified framework when deciding on the use of MPS for restoration and resilience services.
- The minimum DS restoration time is directly related to the repair time of the damaged branches in the DS, irrespective of the model (**MSO-MRT** or **MSO-MPL**) used. If the repair time for damaged branches in the DS exceeds a threshold, the results demonstrated that a full DS restoration may not be achieved. This highlights the necessary adjustments and reinforcements needed to strengthen the response and recovery process when the repair time is uncertain or estimated to be longer than expected (e.g., unavailability or inaccessibility of damaged equipment, shortage in RC workforce).
- The advantage of the proposed MPS technologies over the existing practices prevails under the two formulations investigated. MPS technologies, particularly when their size and capacity increase, can be key to pick up the load at particular nodes and for full DS restoration.

5.2. Limitations and Future Research

This study focused on the solutions for dealing with the aftermath of the HILP incidents (post-disaster) and to enhance the *DS operational resilience*. This study assumes that a certain number of MPS and RC sources are pre-positioned, ready to be optimally dispatched across the TS to help in DS restoration. Future research could study analytics regarding the long-term planning time-horizon to address the investment decision on the MPS resources and for ensuring the *DS structural resilience*.

The conducted tests and numerical evaluations reported in this study are based on the implementation of the proposed **MSO-MRT** and **MSO-MPL** analytics on the IEEE 33-node DS and the 24-node Sioux Falls TS (in Test System 1) as well as the Simplified Electrified TS (in Test System 2). Future research could focus on improvements in the scalability and computational efficiency of the proposed models in large-scale DS (e.g., IEEE 123-node test system) integrated with more realistic TS.

Numerical results indicate that both our models perform well and ensure the efficiency of the service restoration process. Yet one of the models deserves particular attention in that it increasingly relies on the active deployment of MPSs. In crisis conditions, such as during pandemics, when the ability of emergency centers to send maintenance crews is limited, shifting the burden on the machines is a major competitive advantage for decision-makers. Staying on top of recent developments in Industry 4.0 such as self-driving vehicles and adopting such technological breakthroughs may be extremely valuable to ensure service continuity, resilient performance, and customer satisfaction in the future. Advancements in machine learning and artificial intelligence could further facilitate the use of autonomous MPS of the future in harsh environments. A potential future application of MPS is to use aerial means of

transportation particularly in areas with limited or disrupted transportation connectivity and access.

Acknowledgment

The authors are grateful to the editors and to the two anonymous reviewers for their insightful comments and suggestions on earlier versions of this work. This work was supported in part by the National Science Foundation (NSF) under Grants ICER-2022505 and ECCS-2114100, and by grants from the Duke Innovation Fund and the GW Cross Disciplinary Research Fund.

References

Altay, N., W. G. Green III. 2018. OR/MS research in disaster operations management. *Eur. J. Oper. Res.* **175**(1): 475–493.

Angelus, A. 2020. Distributed renewable power generation and implications for capacity investment and electricity prices. *Prod. Oper. Manag.*. Forthcoming.

Arif, A., S. Ma, Z. Wang. 2016. Optimization of transmission system repair and restoration with crew routing. North American Power Symposium (NAPS). 1–6.

Arif, A., Z. Wang, J. Wang, C. Chen. 2017. Power distribution system outage management with cooptimization of repairs, reconfiguration, and DG dispatch. *IEEE Trans. Smart Grid* **9** (5): 4109–4118.

Arif, A., Z. Wang, J. Wang, S. M. Ryan, C. Chen. 2018. Optimizing service restoration in distribution systems with uncertain repair time and demand. *IEEE Trans. Power Syst.* **33**(6): 6828–6838.

Arnette, A. N., C. W. Zobel. 2019. A risk-based approach to improving disaster relief asset prepositioning. *Prod. Oper. Manag.* **28**(2): 457–478.

Balcik, B., S. Silvestri, M. E. Rancourt, G. Laporte. 2019. Collaborative prepositioning network design for regional disaster response. *Prod. Oper. Manag.* **28**(10): 2431–2455.

Baran, M. E., F. F. Wu. 1989. Network reconfiguration in distribution systems for loss reduction and load balancing. *IEEE Power Eng. Rev.* **9**(4): 101–102.

Barrett, D. 2012. Few Big FEMA Generators Humming. Available at https://www.wsj.com/articles/SB10001424052970204707104578093192471666514 (accessed date June 17, 2020).

Bie, Z., Y. Lin, G. Li, F. Li. 2017. Battling the extreme: A study on the power system resilience. *Proc. IEEE* **105**(7): 1253–1266.

Chen, B., C. Chen, J. Wang, K. L. Butler-Purry. 2018. Sequential service restoration for unbalanced distribution systems and microgrids. *IEEE Trans. Power Syst.* **33**(2): 1507–1520.

Chen, B., Z. Ye, C. Chen, J. Wang, T. Ding, Z. Bie. 2019. Toward a synthetic model for distribution system restoration and crew dispatch. *IEEE Trans. Power Syst.* **34**(3): 2228–2239.

Dalenogare, L. S., G. B. Benitez, N. F. Ayala, A. G. Frank. 2018. The expected contribution of Industry 4.0 technologies for industrial performance. *Int. J. Prod. Econ.* **204**: 383–394.

Dehghanian, P. 2017. Power system topology control for enhanced resilience of smart electricity grids. Ph.D. thesis, Texas A&M University.

Ding, T., Z. Wang, W. Jia, B. Chen, C. Chen, M. Shahidehpour. 2020. Multiperiod distribution system restoration with routing repair crews, mobile electric vehicles, and soft-open-point networked microgrids. *IEEE Trans. Smart Grid* **11**(6): 4795–4808.

Faheem, M., S. B. H. Shah, R. A. Butt, B. Raza, M. W. Anwar, M. Ashraf, M. A. Ngadi, V. C. Gungor. 2018. Smart grid communication and information technologies in the perspective of Industry 4.0: Opportunities and challenges. *Comput. Sci. Rev.* **30**: 1–30.

Fortis Alberta. 2019. Removal of RRO Rate Cap Program and What does this Mean for You? Available at https://www.fortisalberta.com/about-us/our-company/blog/fortisalbertablog/2019/08/20/we-explain-the-complex-sophisticated-system-that-brings-electricity-to-you (accessed date June 22, 2020).

Frank, A. G., L. S. Dalenogare, N. F. Ayala. 2019. Industry 4.0 technologies: Implementation patterns in manufacturing companies. *Int. J. Prod. Econ.* **210**: 15–26.

Glover, J. D., M. S. Sarma, T. Overbye. 2012. Power system analysis and design. *Cengage Learning*.

Golari, M., N. Fan, T. Jin. 2017. Multistage stochastic optimization for production-inventory planning with intermittent renewable energy. *Prod. Oper. Manag.* **26**(3): 409–425.

Gupta, S., M. K. Starr, R. Z. Farahani, N. Matinrad. 2016. Disaster management from a POM perspective: Mapping a new domain. *Prod. Oper. Manag.* **25**(10): 1611–1637.

Henry, D., J. E. Ramirez-Marquez. 2016. On the impacts of power outages during hurricane sandy—a resilience-based analysis. *Syst. Eng.* **19**(1): 59–75.

Hermann, M., T. Pentek, B. Otto. 2016. Design principles for Industrie 4.0 scenarios. 49th Hawaii International Conference on System Sciences (HICSS). 3928–3937.

Ivanov, D. 2018. *Structural Dynamics and Resilience in Supply Chain Risk Management*, vol. **265**. Springer International Publishing, Berlin, Germany.

Jamborsalamati, P., M. J. Hossain, S. Taghizadeh, G. Konstantinou, M. Manbachi, P. Dehghanian. 2020. Enhancing power grid resilience through an IEC61850-based EV-assisted load restoration. *IEEE Trans. Industr. Inf.* **16**(3): 1799–1810.

Kahlen, M. T., W. Ketter, J. van Dalen. 2018. Electric vehicle virtual power plant dilemma: Grid balancing versus customer mobility. *Prod. Oper. Manag.* **27**(11): 2054–2070.

Kim, J., Y. Dvorkin. 2018. Enhancing distribution system resilience with mobile energy storage and microgrids. *IEEE Trans. Smart Grid* **10**(5): 4996–5006.

Kuwata, Y., Y. Ohnishi. 2011. Emergency-response capacity of lifelines after wide-area earthquake disasters. *Proc. Int. Symp. Eng. Lessons Learned Great East Jpn. Earthquake* **00**: 1475–1486.

Lavorato, M., J. F. Franco, M. J. Rider, R. Romero. 2012. Imposing radiality constraints in distribution system optimization problems. *IEEE Trans. Power Syst.* **27**(1): 172–180.

Lei, S., J. Wang, C. Chen, Y. Hou. 2016. Mobile emergency generator pre-positioning and real-time allocation for resilient response to natural disasters. *IEEE Trans. Smart Grid* **9**(3): 2030–2041.

Lei, S., C. Chen, Y. Li, Y. Hou. 2019a. Resilient disaster recovery logistics of distribution systems: Cooptimize service restoration with repair crew and mobile power source dispatch. *IEEE Trans. Smart Grid* **10**(6): 6187–6202.

Lei, S., C. Chen, H. Zhou, Y. Hou. 2019b. Routing and scheduling of mobile power sources for distribution system resilience enhancement. *IEEE Trans. Smart Grid* **10**(5): 5650–5662.

Liao, Y., F. Deschamps, E. D. F. R. Loures, L. F. P. Ramos. 2017. Past, present and future of Industry 4.0- A systematic literature review and research agenda proposal. *Int. J. Prod. Res.* **55** (12): 3609–3629.

Lin, Y., B. Chen, J. Wang, Z. Bie. 2019. A combined repair crew dispatch problem for resilient electric and natural gas system considering reconfiguration and DG islanding. *IEEE Trans. Power Syst.* **34**(4): 2755–2767.

Lorca, A., M. Celic, O. Ergun, P. Keskinocak. 2017. An optimization-based decision-support tool for post-disaster debris operations. *Prod. Oper. Manag.* **26**(6): 1076–1091.

National Academies of Sciences. 2017. *Enhancing the Resilience of the Nations Electricity System*. National Academies Press, Washington, D.C..

National Centers for Environmental Information. 2020. Billion-Dollar Weather and Climate Disasters: Overview. Available at https://www.ncdc.noaa.gov/billions/ (accessed date July 3, 2020).

Nguyen, T., S. Wang, M. Alhazmi, M. Nazemi, A. Estebsari, P. Dehghanian. 2020. Electric power grid resilience to cyber adversaries: State of the art. *IEEE Access* **8**: 87592–87608.

Ni, W., J. Shu, M. Song. 2018. Location and emergency inventory pre-positioning for disaster response operations: Min-max robust model and a case study of Yushu earthquake. *Prod. Oper. Manag.* **27**(1): 160–183.

Olsen, T. L., B. Tomlin. 2020. Industry 4.0: Opportunities and challenges for operations management. *Manuf. Serv. Oper. Manag.* **22**(1): 113–122.

Pan, X., M. Dresner, M. Mantin, J. A. Zhang. 2020. Pre-hurricane consumer stockpiling and posthurricane product availability: Empirical evidence from natural experiments. *Prod. Oper. Manag.* **29**(10): 2350–2380.

Panteli, M., P. Mancarella. 2015. The grid: Stronger, bigger, smarter?: Presenting a conceptual framework of power system resilience. *IEEE Power Energ. Mag.* **13**(3): 58–66.

Parker, G. G., B. Tan, O. Kazan. 2019. Electric power industry: Operational and public policy challenges and opportunities. *Prod. Oper. Manag.* **28**(11): 2738–2777.

Qi, W., Z. J. M. Shen. 2019. A smart-city scope of operations management. *Prod. Oper. Manag.* **28**(2): 393–406.

Rada, M. 2015. Industry 5.0 - from Virtual to Physical. Available at https://www.linkedin.com/pulse/industry-50-from-virtual-physical-michael-rada (accessed date June 5, 2020).

Schwab, K. 2017. *The Fourth Industrial Revolution*. Currency, Redfern, NSW.

Schwertner, K., P. Zlateva, D. Velev. 2018. Digital technologies of Industry 4.0 in management of natural disasters. In: *Proceedings of the 2nd International Conference on E-commerce, E-Business and E-Government*95–99.

Smith, A.B. 2020. 2010–2019: A Landmark Decade of U.S. Billion-Dollar Weather and Climate Disasters. Available at https://www.climate.gov/news-features/blogs/beyond-data/2010-2019-landmark-decade-us-billion-dollar-weather-and-climate (accessed date July 6, 2020).

Sodhi, M.S., C. S. Tang. 2014. Buttressing supply chains against floods in Asia for humanitarian relief and economic recovery. *Prod. Oper. Manag.* **23**(6): 938–950.

Stauffer, J. M., S. Kumar. 2021. Impact of incorporating returns into pre-disaster deployments for rapidonset predictable disasters. *Prod. Oper. Manag.* **30**(2): 451–474.

Tang, C. S., L. P. Veelenturf. 2019. The strategic role of logistics in the Industry 4.0 era. *Transport. Res. Part E Logist. Transport. Rev.* **129**: 1–11.

Ukkusuri, S. V., W. F. Yushimito. 2009. A methodology to assess the criticality of highway transportation networks. *J. Transport. Secur.* **2**(1-2): 29–46.

Valogianni, K., W. Ketter, J. Collins, D. Zhdanov. 2020. Sustainable electric vehicle charging using adaptive pricing. *Prod. Oper. Manag.* **29**(6): 1550–1572.

Wang, L., M. Torngren, M. Onori. 2015. Current status and advancement of cyber-physical systems in manufacturing. *J. Manuf. Syst.* **37**: 517–527.

Wei, W., W. U. Danman, W. U. Qiuwei, M. Shafie-Khah, J. P. Catalao. 2019. Interdependence between transportation system and power distribution system: A comprehensive review on models and applications. *J. Modern Power Syst. Clean Energy* **7** (3): 433–448.

Xu, Y., Y. Wang, J. He, M. Su, P. Ni. 2019. Resilience-oriented distribution system restoration considering mobile emergency resource dispatch in transportation system. *IEEE Access* **7**: 73899–73912.

Yang, Z., P. Dehghanian, M. Nazemi. 2020. Seismic-resilient electric power distribution systems: Harnessing the mobility of power sources. *IEEE Trans. Ind. Appl.* **56**(3): 2304–2313.

Yao, S., P. Wang, P. Liu, H. Zhang, T. Zhao. 2019. Rolling optimization of mobile energy storage fleets for resilient service restoration. *IEEE Trans. Smart Grid* **11**(2): 1030–1043.

Ye, Y. W. Jiao, H. Yan. 2020a. Managing relief inventories responding to natural disasters: Gaps between practice and literature. *Prod. Oper. Manag.* **29**(4): 807–832.

Ye, Z., C. Chen, B. Chen, K. Wu. 2020b. Resilient service restoration for unbalanced distribution systems with DERs by leveraging mobile generators. *IEEE Trans. Industr. Inf.* **17**(2): 1386–1396.

Zare, M., F. Kamranzad, I. Parcharidis, V. Tsironi. 2017. Preliminary report of mw7.3 Sarpol-e Zahab, Iran earthquake on November 12, 2017. *EMSC Report 1–10*.

Zhang, B., P. Dehghanian, M. Kezunovic. 2019. Optimal allocation of PV generation and battery storage for enhanced resilience. *IEEE Trans. Smart Grid* **10**(1): 535–545.

Zhang, G., F. Zhang, X. Zhang, K. Meng, Z. Y. Dong. 2020. Sequential disaster recovery model for distribution systems with co-optimization of maintenance and restoration crew dispatch. *IEEE Trans. Smart Grid* **11**(6): 4700–4713.

Supporting Information

Additional supporting information may be found online in the Supporting Information section at the end of the article.

Appendix A: Power Distribution System with Radial Topology.

Appendix B: Nomenclature.

Appendix C: Test Scenarios and Numerical Results: Test System 2.